Title

The mitochondrial BK_{Ca} channel cardiac interactome reveals BK_{Ca} association with the mitochondrial import receptor subunit Tom22, and the adenine nucleotide translocator.

Authors

Zhang, Jin
Li, Min
Zhang, Zhu
et al.

Publication Date

2017-03-01

DOI

10.1016/j.mito.2016.08.017

Peer reviewed

HHS Public Access

Author manuscript

Mitochondrion. Author manuscript; available in PMC 2018 March 01.

Published in final edited form as:

Mitochondrion. 2017 March ; 33: 84–101. doi:10.1016/j.mito.2016.08.017.

The mitochondrial BK_{Ca} channel cardiac interactome reveals BK_{Ca} association with the mitochondrial import receptor subunit Tom22, and the adenine nucleotide translocator

Jin Zhang[a,c], **Min Li**[a], **Zhu Zhang**[a], **Ronhui Zhu**[a], **Riccardo Olcese**[a,b,d,e,*], **Enrico Stefani**[a,b,d,e,*], and **Ligia Toro**[a,c,d,e,*]

[a]Department of Anesthesiology, Division of Molecular Medicine, University of California, Los Angeles, Los Angeles, CA, USA.

[b]Department of Physiology, University of California, Los Angeles, Los Angeles, CA, USA.

[c]Department of Molecular & Medical Pharmacology, University of California, Los Angeles, Los Angeles, CA, USA.

[d]Brain Research Institute, University of California, Los Angeles, Los Angeles, CA, USA.

[e]Cardiovascular Research Laboratory, University of California, Los Angeles, Los Angeles, CA, USA.

Abstract

Mitochondrial BK_{Ca} channel, mitoBK_{Ca}, regulates mitochondria function in the heart but information on its protein partnerships in cardiac mitochondria is missing. A directed proteomic approach discovered the novel interaction of BK_{Ca} with Tom22, a component of the mitochondrion outer membrane import system, and the adenine nucleotide translocator (ANT). The expressed protein partners co-immunoprecipitated and co-segregated into mitochondrial fractions in HEK293T cells. The BK_{Ca} 50 amino acid splice insert, DEC, facilitated BK_{Ca} interaction with ANT. Further, BK_{Ca} transmembrane domain was required for the association with both Tom22 and ANT. The results serve as a working framework to understand mitoBK_{Ca} import and functional relationships.

Keywords

Proteomics; BK channel; MaxiK channel; potassium ion channel; mitochondria; heart; Tom22; adenine nucleotide translocator; macromolecular complex

Address correspondence to: Dr. Ligia Toro, Department of Anesthesiology, UCLA School of Medicine, BH-509A CHS, Box 957115, Los Angeles, CA 90095-7115, Phone: 1 (310) 709 5204, FAX: 1 (310) 825 5379, ltoro@ucla.edu.

*Co-senior authors

1. Introduction

Mitochondrial BK_{Ca} channels ($mitoBK_{Ca}$) are safeguards of cardiac function as their activation protects the heart from ischemic insult, a property that is absent in the knockout animal (Xu et al., 2002; Singh et al., 2013; Soltysinska et al., 2014). One of the proposed mechanisms by which $mitoBK_{Ca}$ activation favors cardiac health after ischemic insult is via improved mitochondrial Ca^{2+} handling and regulation of the mitochondrial permeability transition pore (mPTP) (Singh et al., 2013). Consistent with this idea, in other systems, $mitoBK_{Ca}$ pharmacological inhibition produces cytochrome *c* release, an event associated with the opening of the mPTP and cell death; while Bax (proapoptotic Bcl-2 associated protein X), a mPTP activator, inhibits channel activity (Cheng et al., 2011). In agreement with its protective role, the activation of cardiac $mitoBK_{Ca}$ improves basal mitochondrial energetic performance (Aon et al., 2010), whereas silencing BK_{Ca} expression reduces cardiac oxidative phosphorylation (Soltysinska et al., 2014).

To exert its function in mitochondria, $mitoBK_{Ca}$ must be first transported into this organelle and likely associate with partner proteins, as it does in other regions of the cell (Toro et al., 2013). Supporting this view, a two-hybrid system approach discovered that the regulatory β1 subunit of BK_{Ca} channels directly binds to a mitochondrial protein, cytochrome *c* oxidase subunit I (Ohya et al., 2005).

We have previously demonstrated that the $mitoBK_{Ca}$ pore-forming α subunit is encoded by the same gene that encodes the plasma membrane BK_{Ca} channel, *Kcnma1,* and that a 50 amino acid C-terminal splice insert (named DEC) favors BK_{Ca} channel targeting into mitochondria of adult cardiomyocytes (Singh et al., 2013). Thus, the overall structure of the $mitoBK_{Ca}$ channel is equivalent to that of the well-studied plasma membrane tetrameric channel, with each α-subunit composed of 7 transmembrane segments (S0-S6), a long intracellular C-terminus and an extracellular N-terminus (Meera et al., 1997). However, the protein partners of $mitoBK_{Ca}$ are unknown.

Efforts to identify BK_{Ca} channel partners at a large scale have been few and restricted to cochlea and brain preparations (Kathiresan et al., 2009; Gorini et al., 2010; Sokolowski et al., 2011; Singh et al., 2016). In this work, we have examined the interactome of $mitoBK_{Ca}$ in adult heart (isolated cardiomyocytes and whole ventricle), using a directed proteomic approach aided by co-immunoprecipitation with BK_{Ca} antibodies and pull-down with recombinant DEC sequence. Two putative protein partners were selected to validate and further examine the regions in BK_{Ca} involved in the associations: i) Tom22 from the mitochondrial import system, and ii) the adenine nucleotide translocator (ANT), which is linked to oxidative phosphorylation and the regulation of mPTP.

2. Materials and methods

2.1. Animals

Sprague-Dawley male rats (3 months old) were used. Protocols received institutional approval.

2.2. Antibodies

The following antibodies were used: Anti-BK_{Ca} monoclonal antibody (mAb) (75-022, UC Davis/ NIH NeuroMab facility), Anti-BK_{Ca} polyclonal (p) Ab (APC-021, Alomone Labs), Anti-c-Myc mAb (M4439, Sigma), Anti-c-Myc polyclonal pAb (C3956, Sigma), Anti-HA mAb (H3663, Sigma), Anti-HA pAb (H6908, Sigma), anti-DDK mAb (TA50011, OriGene), Goat Anti-Rabbit IgG Alexa Fluor® 680 conjugate (A21109, Invitrogen), and IRDye® 800CW Goat Anti-Mouse IgG (926-32210, Odyssey).

2.3. Clones

Full length human BK_{Ca} α-subunit starting from Met1 (BK_{Ca}) with or without DEC splice insert (EKKWFTDEPD NAYPRNIQIK PMSTHMANQI NQYKSTSSLI PPIREVEDEC) at the C-terminus were used in all experiments except for Figs. 4, 5 and 7 (see below). Compared to NCBI Accession No. U11058.2 (Wallner et al., 1995), which starts from Met3, constructs starting from Met1 have additional 96 amino acids at the N-terminus that includes a 3xHemagglutinin (HA)-tag upstream Met3 (MANGGGGGGG SSGGGGGGGG SSLRMSSNIH ANHLSLDASS SSSSSSSSSS SSSSSSSSSS VHEPK*MYPYD VPDYAGYPYD VPDYAGSYPY DVPDYA*; 3xHA tag sequences are in italics). BK_{Ca}-DEC has the C-terminal DEC sequence inserted downstream amino acids RDKQN as found in the heart (Singh et al., 2013). Clones starting from Met3 (Accession No. U11058.2) were either untagged or tagged at the N-terminus with c-Myc epitope (Meera et al., 1997) (Figs. 4 and 7) or with HA epitope (Fig. 5). Clones used in deletion constructs experiments (Figs. 4 and 7) were: BK_{Ca} (1-1113); C-terminal deletion constructs 1-343, 1-441 and 1-711; and N-terminal deletion constructs 322-1113 and 679-1113; numbers correspond to NCBI Accession No. U11058.2. All BK_{Ca} constructs were in pcDNA3. Tom22 construct was the human translocase of outer mitochondrial membrane 22 homolog (Accession No. NM_020243.4) with C-terminal c-Myc and DDK tags in pCMV6. ANT construct was the human mitochondrial adenine nucleotide translocator (Accession No. NM_001151.2) with a C-terminal c-Myc-DDK tag in pCMV6. Tom 22 and ANT clones were purchased from OriGene Technologies (Rockville, MD).

2.4. Expression of recombinant fusion proteins in *E. Coli*

Glutathione *S*-Transferase (GST)-DEC and GST in pGEX3 vector were transformed into *E. coli* BL21DE3 (Invitrogen) and cultured at 37 °C using Luria-Bertani (LB) broth (Thermo Fisher Scientific) supplemented with 100 ng/mL ampicillin until OD_{600}= 0.5. The expression of GST-DEC and GST was then induced by adding IPTG to a final concentration of 0.2 mM. Cultures were continued in a rotary shaker for 4 h at 37°C. Bacteria were centrifuged at 1000 g for 5 min to collect the pellet. The pellet was further lysed using sonication (15 s) at power level 2 in lysis buffer (mM): 50 Tris, pH 7.4, 100 NaCl, 5 $MgCl_2$, 1% Triton X-100, 10% glycerol, supplemented with fresh 2 mM DTT, 200 mM PMSF and 1:500 dilution of protease inhibitor cocktail (11697498001, Roche).

2.5. Isolation of cardiomyocytes from left ventricle

Sprague-Dawley rats were anesthetized and injected with heparin (200 IU/kg, i.v.). After 15 min hearts were harvested in ice-cold Tyrode's solution (mM): 130 NaCl, 5.4 KCl, 1 $MgCl_2$,

0.6 Na_2HPO_4, 10 glucose, 5 taurine, 10 2,3-butanedione monoxime, and 10 HEPES, pH 7.4, oxygenated with 95% O_2-5% CO_2 (v/v), and mounted on a modified Langendorff apparatus with an 80 cm H_2O constant pressure. After 5-10 min of perfusion with Tyrode's solution at 37°C, the hearts were next perfused for 15 min with Tyrode's solution containing 372 U/mL Collagenase Type-2 and 1.0 U/mL Protease Type-XIV, and washed for 10-15 min with KB solution (mM): 25 KCl, 10 KH_2PO_4, 5 creatine, 2 $MgSO_4$, 20 glucose, 20 taurine, 100 K-glutamate, 10 aspartic acid, 5 HEPES, 0.5 EGTA, and 1% (wt/v) BSA, pH 7.2 oxygenated with 95% O_2-5% CO_2 (v/v). After washing, the left ventricles were tweezed into pieces in KB solution to release cells. Isolated cardiomyocytes were filtered through a 100 μm strainer, and centrifuged at 1,000 g for 2 min.

2.6. Isolation of "crude" mitochondria and Percoll-purification

i) "Crude" mitochondria. Isolated cardiomyocytes or left ventricles were homogenized with a Potter-Elvehjem homogenizer (20 rapid strokes) on ice and using isolation buffer A (mM): 70 sucrose, 210 mannitol, 50 Tris-HCl, and 1 Na_2-EDTA, pH 7.4. The homogenate was centrifuged at 2,400 g for 5 min at 4°C. The supernatant was then centrifuged at 17,000 g for 10 min at 4°C. The pellet containing "crude" mitochondria was either further purified (ventricle samples) using Percoll gradient or directly resuspended in lysis buffer (isolated cardiomyocyte samples) (section **2.7**). ii) Percoll purification. "Crude" mitochondria was carefully added onto 3 mL of 30% (v/v) Percoll (Graham , 2001) in buffer B (mM): 250 sucrose, 10 Na-HEPES, 1 Na_2-EDTA, pH 7.4. Samples were centrifuged in a fixed angle rotor at 50,000 g for 45 min. After ultracentrifugation, three clear layers were observed, and labeled as M1, M2 and M3 (Singh et al., 2012). The M3 fraction, corresponding to the purified mitochondria, was carefully isolated and resuspended in 1 mL of isolation buffer A and centrifuged at 17,000 g for 10 min. The pellet was washed twice by resuspension with the same buffer and centrifuged again at 17,000 g for 5 min each. The purified mitochondria were lysed within 2 h after isolation.

2.7. Mitochondria and cardiomyocyte lysates

Mitochondria or isolated cardiomyocyte preparations were incubated at 4°C (on a rotatory shaker for 1 h) in cell lysis buffer (1 and 3 mL, respectively) (mM): 50 Tris, 150 NaCl, 5 EDTA, 0.1% Nonylphenyl Polyethylene Glycol (NP-40 alternative, Calbiochem), and 0.25% Na-deoxycholate, pH 7.4 supplemented with protease inhibitor cocktail (one tablet/50 mL) and 200 mM PMSF. After lysis, samples were centrifuged at 17,000 g for 10 min at 4 °C and the supernatant was saved at −80°C for future use. Protein concentration was measured with Bio-Rad Protein Assay method.

2.8. Pull down assay and SDS-PAGE

Recombinant fusion protein GST-DEC and GST (control) were used. Glutathione Sepharose 4B beads (GE healthcare) were first prewashed with bacteria lysis buffer and then incubated with 3 mg of GST or GST-DEC on a rotatory shaker at 4 °C for 3 h. After binding of GST-DEC and GST onto Glutathione Sepharose 4B beads, each sample was further washed with bacteria lysis buffer 3 times, following incubation with 2 mg protein of cardiomyocyte cell lysates or mitochondrial lysates on a rotatory shaker at 4 °C for 2 h. Each sample was then

incubated with SDS loading buffer for 1 h at 37 °C and centrifuged at 10,000 g for 3 min. The supernatant was separated on a 4-20% SDS-PAGE at room temperature. The protein bands were stained with SYPRO-RUBY stain according to the manufacturer's instructions (Bio-Rad).

2.9. Immunoprecipitation for proteomics

Mitochondrial lysates (see section **2.7**) were precleared with 10 μL protein A/G resin/mg protein (Pierce Biotechnology Inc.) for 1 h at 4 °C. Next, samples were centrifuged at 2,400 g for 5 min at 4 °C to remove protein A/G resin. The supernatant was collected, and the protein concentration was calculated according to the Bio-Rad method. Anti-BK_{Ca} antibodies (2 μg) or IgGs (2 μg, control) were incubated for 2 h at 4 °C with 10 μL protein A/G resin on a rotatory shaker. Unbound antibodies were then removed by centrifugation 5 times at 2,400 g for 1 min at 4 °C. Mitochondria lysates (2 mg protein each) were added to immobilized anti-BK_{Ca} and IgG antibodies, and incubated on a rotatory shaker overnight at 4 °C. Samples were washed 5 times with cell lysis buffer at 2,400 g for 1 min each at 4 °C. Laemmli sample buffer (30 μL of 3X buffer) was added, and samples were incubated at 37 °C for 1 h. Eluted proteins were centrifuged at 17,000 g for 10 min at 4 °C, and separated on a 4-20% SDS-PAGE at room temperature. Protein bands were then stained with SYPRO-RUBY.

2.10. Mass spectrometry analysis of proteins

Plugs of SYPRO-RUBY stained 1-D gels containing GST- and GST-DEC bound proteins or anti-BK_{Ca} and IgG bound proteins were excised using a sterile scalpel blade. Sections (~2 mm) ranging from 10 kDa to 250 kDa were collected and further digested with trypsin. Protein digestion and elution were carried as described earlier (Singh et al., 2009; Singh et al., 2013). Liquid chromatography, mass spectrometry in tandem (LC/MS/MS) was performed using a Thermo LTQ-Orbitrap XL mass spectrometer equipped with an Eksigent Nano Liquid chromatography-1D plus system and an Eksigent auto sampler at the University of California Los Angeles W. M. Keck Proteomic Center. Sequences were assigned using the Swiss-Prot Rat database and the MASCOT Daemon search engine. The output data included MASCOT score, molecular weight, number of peptides matched, peptide sequences, sequence coverage, rank, and p-value. To select candidate proteins, the score value of individual spectra was set at a 95% confidence level and a MASCOT score > or =21. Peptides were selected as specified by the Peptide Prophet algorithm. GST-DEC or BK_{Ca} specific interacting proteins were defined as those not found in the samples using GST alone or IgG, respectively.

2.11. Cell culture

HEK293T cells were cultured in Dulbecco's Modified Eagle Medium (DMEM, Gibco) supplemented with 10% (v/v) FBS, 2 units/mL streptomycin and penicillin at 37 °C in a humidity-controlled CO_2 [5% (v/v)] incubator.

2.12. Transient transfection

HEK293T cells were transfected at 70% confluence using Lipofectamine 2000 (Invitrogen) following the manufacturer's instructions. Plasmid DNAs were incubated with Lipofectamine 2000 in OPTI-MEM (Invitrogen) for 20 min at room temperature (20-25 °C). Plasmid-Lipofectamine mixtures were then incubated with cells in OPTI-MEM at 37 °C in a CO_2 incubator for 5-7 h. Afterwards, DMEM containing 20% FBS was added to reach a final FBS concentration of 10%. Because cotransfection of Tom22 or ANT with BK_{Ca} significantly decreased the expression of BK_{Ca}, we first transfected BK_{Ca} constructs to allow their expression followed by a second transfection of Tom22 or ANT 24 h later. All constructs were transfected with 10 μg plasmid/100 mm dish with the exception of Tom22 that was transfected at 1 μg plasmid/100 mm dish in experiments involving truncated BK_{Ca} channels. After 48 h from the second transfection, cells were collected and lysed for further analysis.

2.13. Western blot

HEK293T cells or cellular fractions were treated with cell lysis buffer (see section **2.7**) containing protease inhibitor cocktail (one tablet/50 mL), and incubated for 30 min at 4 °C with shaking. Samples were then centrifuged at 17,000 g for 10 min at 4 °C, and the supernatant was collected as lysates. Lysate proteins (20 μg/lane) were separated on 4–20% SDS/PAGE and transferred to nitrocellulose membranes. Nitrocellulose membranes were blocked with 5% (wt/v) milk in TBS (150 mM NaCl, 20 mM Tris-HCl, pH 7.4) at room temperature for 60 min and incubated with antibodies (2 μg/mL) overnight. Next day, membranes were washed 3 times with TBS and incubated with 0.01 μg/mL secondary Abs for 1 h at room temperature. After washing 3 times, membranes were visualized and scanned with the Odyssey Imaging System (Li-Cor Biosciences).

2.14. Co-immunoprecipitation of heterologously expressed proteins

HEK293T cells expressing different combinations of BK_{Ca} constructs, Tom22 or ANT were cultured on 100 mm dish and lysed with cell lysis buffer containing protease inhibitor cocktail. Lysates were centrifuged at 17,000 g for 10 min at 4 °C and the supernatant was cleared with 10 μL protein A/G resin/mg protein for 1 h at 4 °C on a rotatory shaker. The precleared lysates (1 mg protein) were incubated with 10 μL protein A/G resin preconjugated with 2 μg antibodies (Anti-HA mAb or anti-BK_{Ca} mAb for BK_{Ca} and BK_{Ca}-DEC; anti-c-Myc mAb for Tom22, ANT, and BK_{Ca} constructs; anti-DDK mAb for Tom22 and ANT; and Flag pAb for ANT) in a total volume of 500 μL overnight at 4 °C. After incubation, samples were centrifuged at 2,400 g for 1 min and washed for 5 times with cell lysis buffer. The proteins were eluted from the beads with 30 μL 3X Laemmli sample buffer at 37 °C for 1 h. After elution, samples were centrifuged at 17,000 g for 10 min at 4°C and separated on 4-20% SDS-PAGE along with whole cell lysates. Separated proteins were transferred to nitrocellulose membranes and immunoblotted with respective antibodies (1 μg/mL). Single- or double-labeled immunoblots were imaged as described above.

2.15. Cell fractionation

HEK293T cells were collected and homogenized in isolation buffer A (mM): 70 sucrose, 210 mannitol, 1 Na_2-EDTA, 50 Tris-HCl, pH 7.4 using a Potter-Elvehjem homogenizer (3 rapid strokes). The homogenate was centrifuged at 2,400 g for 5 min in an Eppendorf tube. The supernatant was collected and centrifuged at 17,000 g for 10 min. The pellet containing "crude" mitochondria was resuspended in 50 μL of isolation buffer A, and the supernatant was kept. The "crude" mitochondria preparation was further purified by Percoll gradient centrifugation (see section **2.6**) and lysed within 2 h after isolation. The supernatant after isolating the "crude" mitochondria was used to isolate the "crude" membrane fraction and cytosolic fraction. The supernatant was centrifuged in the same fixed angle rotor at 100,000 g for 30 min. The pellet was collected as "crude" membrane fraction. The supernatant containing ribosomes and cytosol was named here cytosolic fraction. All fractions were lysed in cell lysis buffer (see section **2.7**) for Western blot analysis together with whole-cell lysate.

2.16. Statistics

Data are presented as means ± S.E. Statistical comparisons between groups were made using Student's *t* test. Multiple comparisons were done with ANOVA followed by the Tukey test. A p value<0.05 was considered statistically significant. All experiments were performed using at least three independent preparations.

3. Results

3.1. Identification of mitoBK$_{Ca}$-associated cardiac mitochondrial proteins

mitoBK$_{Ca}$-associated proteins were identified using a directed proteomic approach using recombinant GST-DEC and specific anti-BK$_{Ca}$ mAb (Misonou et al., 2006). The BK$_{Ca}$ C-terminal DEC insert is known to support BK$_{Ca}$ mitochondrial expression in adult cardiomyocytes (Singh et al., 2013), and thus, was expected to associate with mitochondrial partners. Three protocols were used to maximize the isolation of BK$_{Ca}$ protein partners: 1) pull down from "crude" mitochondria of isolated cardiomyocytes using GST-DEC and GST (control); 2) pull down from Percoll-purified mitochondria of left ventricle using anti-BK$_{Ca}$ mAb and IgG (control); and 3) pull down from whole cardiomyocytes with GST-DEC and GST (control).

The "crude" mitochondria preparation had the advantage of using solely rat cardiomyocytes. However, due to material limitations, further Percoll purification of this preparation was impractical; instead, we used the GST-DEC fusion protein that, we expected, would favor specific recognition of mitochondrial proteins. To identify proteins interacting with BK$_{Ca}$ regions other than DEC, we used a specific BK$_{Ca}$ mAb to immunoprecipitate proteins from the Percoll-purified mitochondria. We also investigated whether GST-DEC could pick up mitochondrial interacting proteins in whole ventriculocyte lysates. Indeed, with this approach using the whole ventriculocyte lysates with GST-DEC as bait yielded 49 mitochondrial partners out of a total of 341 partners (~14% mitochondrial proteins; in 3 independent experiments). This result is consistent with experiments using: i) GST-DEC to pull down proteins in "crude" mitochondria from isolated cardiomyocytes that revealed 68

mitochondrial partners out of a total of 561 partners (~12% mitochondrial proteins; in 3 independent experiments), and ii) anti-BK_{Ca} mAb to immunoprecipitate proteins from Percoll-purified mitochondria from left ventricle that detected 77 mitochondrial partners out of a total of 428 partners (~17%; in 3 independent experiments). Overall, a total of 1079 different proteins were identified as partners of BK_{Ca} in cardiomyocytes and left ventricle using the above mentioned protocols. The locations were catalogued into intracellular organelles i.e. mitochondrion (151 proteins), endoplasmic reticulum (44 proteins), Golgi (17 proteins), and nucleus (151 proteins) (Tables 1 and 2); cytoplasm (322 proteins); and plasma membrane (223 proteins). The remaining 171 proteins were catalogued as "others" by the UniProt Knowledgebase.

In this work, we focused our analysis on the 151 mitochondrial proteins (Table 1). A functional annotation analysis of these proteins using the bioinformatic tool **D**atabase for **A**nnotation, **V**isualization and **I**ntegrated **D**iscovery (DAVID) revealed that BK_{Ca} channel is associated with 13 distinctive biological processes in the mitochondria (Fig. 1A). Among those, of special interest were import mechanisms (8 proteins), oxidative phosphorylation (28 proteins), transport (7 proteins), TCA cycle (9 proteins), fatty acid metabolism (5 proteins), and programmed cell death (8 proteins). As an example, a mass spectrum obtained for the adenine nucleotide translocator, ANT is given in Fig. 1B. The uncovered relationship between BK_{Ca} channel and the predicted biological activities underscores the potential role of BK_{Ca} channel in contributing to the functional integrity of mitochondria and consequently of cardiac cells.

3.2. mitoBK_{Ca} interacts with Tom22 in HEK293T cells

One of the partners found in the interactome associated with the DEC sequence was Tom22 (matching peptide LQMEQQQQLQQR; Table 1), a protein located on the outer mitochondrial membrane. Tom22 is known to serve as an initial recognition site for protein import into mitochondria (Mayer et al., 1995). Thus, we deemed it important to corroborate its association with BK_{Ca} as this would permit to start setting the building blocks of mitoBK_{Ca} import pathway. Thus, we co-expressed BK_{Ca} with or without DEC (3HA-tagged N-terminal of Met3) with Tom22 (C-terminal c-Myc tagged) in HEK293T cells for co-immunoprecipitation analysis by immunoprecipitating BK_{Ca} or BK_{Ca}-DEC and examining the immunoprecipitation products for Tom22. As controls, we also expressed each protein alone.

Figure 2A shows in the same blot the immunoprecipitation of BK_{Ca} and BK_{Ca}-DEC together with the successful co-immunoprecipitation of Tom 22 by both BK_{Ca} variants. In separate experiments, immunoprecipitation of Tom22 yielded bands of similar sizes as the ones observed in the co-immunoprecipitation products confirming Tom22 molecular size (not shown). The strong signal near 100 kDa likely corresponds to IgG composite or non-specific labeling of the secondary antibody. The specificity of the co-immunoprecipitation was confirmed by reverse coimmunoprecipitation with BK_{Ca} (*see* section 3.4). Fig. 2B demonstrates in the same blot the proper expression of each clone in the input lysates. The co-immunoprecipitation (Co-IP) efficiency of the two BK_{Ca} variants was calculated as previously described (Li et al., 2013) by the ratio of the band intensities of co-

immunoprecipitated Tom22 (as in Fig. 2A, squares) to those of immunoprecipitated BK_{Ca} variant (as in Fig. 2A, arrows), and normalized to the corresponding Tom22 signals in the input lysates (as in Fig. 2B, arrowhead). Figure 2C shows the mean values demonstrating that BK_{Ca} and BK_{Ca}-DEC had a similar ability to interact with Tom22 (0.89±0.18 vs. 0.91±0.15; n=3 each). These results are consistent with the proteomic data and demonstrate that Tom22 association with BK_{Ca} in HEK293T cells does not depend on the presence of DEC sequence in BK_{Ca}.

3.3. Both mitoBK_{Ca} and Tom22 are imported into mitochondria of HEK293T cells

We next examined the subcellular localization of co-expressed Tom22 and BK_{Ca} through cell fractionation and immunoblotting. Figure 3A,B (upper panels) and Fig. 3C,D show that both BK_{Ca} and BK_{Ca}-DEC were significantly enriched in the "crude" mitochondria fraction (Cmito). Importantly, BK_{Ca} isoforms were also detected in the purified mitochondria fraction (Pmito), indicating that BK_{Ca} was imported into mitochondria in HEK293T cells. Interestingly, Tom22 was found in all of the fractions examined (A,B, bottom panels; E) including the cytosol and crude membranes. This finding cannot be explained by inadequate separation since, as shown later in section 3.6, a typical mitochondrial marker, ANT, was only present in "crude" and purified mitochondrial fractions. The mean relative abundance values of BK_{Ca} and BK_{Ca}-DEC in Fig. 3C,D show a very similar pattern of expression in the different subcellular fractions. Both variants gave the strongest signal in "crude" mitochondria (BK_{Ca}=1.62±0.13 and BK_{Ca}-DEC=1.26±0.11, n=3 each) suggesting that the majority of BK_{Ca} channels were localized to mitochondria or in mitochondria-associated membranes. In agreement, the purified mitochondria fraction displayed a considerable amount of BK_{Ca} channel signal (BK_{Ca}=0.73±0.09, BK_{Ca}-DEC=0.45±0.17, n=3, each). As expected from previous studies (Ma et al., 2007) both variants were also present in "crude" membranes (BK_{Ca}=0.36±0.07, BK_{Ca}-DEC=0.65±0.20, n=3 each), whereas their presence in the cytosolic fraction was minimal (BK_{Ca}=0.02±0.03, BK_{Ca}-DEC=0.02±0.001, n=3 each).

The mean relative quantification of Tom22 in different fractions is shown in Fig. 3E. As stated earlier, Tom22 distribution spanned all fractions examined. Nevertheless, the expression and distribution of Tom22 in the "crude" mitochondria (0.94±0.20, n=6 each) and the purified mitochondria (0.59±0.25, n=6 each) was robust. Thus, the results indicate that both BK_{Ca} variants and Tom22 are targeted into mitochondria, though not exclusively, in HEK293T cells.

3.4. The BK_{Ca} channel interacts with Tom22 through its transmembrane region

To identify the regions in BK_{Ca} channel relevant for its association with Tom22, we performed coimmunoprecipitations with BK_{Ca} N- and C-terminal deletions. Figure 4A shows a scheme of wild-type BK_{Ca} (1-1113 amino acids) where the arrows delineate the regions spanned by each construct (the numbers correspond to the amino acids numbering). All BK_{Ca} constructs were tagged with c-Myc epitope at the N-terminus. C-terminal truncates were: 1-343, 1-441 and 1-711; N-terminal deletion constructs were: 322-1117 covering the whole C-terminus and 679-1113 that includes the regulator for potassium conductance 2 (RCK2) domain, also called the "tail" region. Tom22 contained a DDK tag at the C-terminus. HEK293T cells were transfected with BK_{Ca} constructs alone (control) or in

conjunction with Tom22, and with Tom22 alone (control). All samples were subjected to immunoprecipitation using anti-DDK mAb targeting Tom22, and different truncated BK_{Ca} proteins were detected with anti-c-Myc pAb (Fig. 4B, top). The co-immunoprecipitated signals of 1-343, 1-441, and 1-711 constructs were strong (lanes 8-10, solid squares) compared to the background signals of BK_{Ca} proteins expressed alone (lanes 1-3, dashed squares), whereas co-immunoprecipitated C-terminus (322-1113) and "tail" (679-1113) were barely detected (lanes 11,12, solid squares) and practically absent in the control (lanes 4 and 5, dashed squares). As reference, lane 13 shows the co-immunoprecipitated wild type BK_{Ca}. Note that this coimmunoprecipitation corresponds to the reverse coimmunoprecipitation of Fig. 2A. Figure 4B (bottom panel) shows the successful immunoprecipitation of Tom22 for the same experiment, and Fig. 4C displays the expression of all clones in the input lysates. The co-immunoprecipitation (co-IP) efficiency of different BK_{Ca} regions was calculated by first subtracting the corresponding background signals from the coimmunoprecipitation signals of BK_{Ca} constructs (as in Fig. 4B, top) and normalizing to the corresponding immunoprecipitated Tom22 (as in Fig. 4B, bottom) and BK_{Ca} input signals (as in Fig. 4C, top, lanes 8-13). The co-IP efficiency value of wild-type BK_{Ca} was set to 1. Constructs 1-343, 1-441, and 1-711 showed a similar ability to interact with Tom22 (1-343=3.43±0.90, 1-441= 2.42±0.60, 1-711=2.04±0.42; n=3 each, $p>0.05$), which is much higher than that observed for wild-type BK_{Ca}. In contrast, both the C-terminus and tail lost their ability to efficiently coimmunoprecipitate Tom22 (C-terminus=0.33±0.05, tail=0.42±0.21; n=3 each). Note that although construct 1-711 contains part of the C-terminus (up to the first amino acids of the "tail" segment) it maintained a significant interaction with Tom22. Taken together, the results suggest that the interaction between BK_{Ca} channel and Tom22 is mainly through the transmembrane domain of BK_{Ca} channel and that the "tail" region exerts an inhibitory action on the association of both proteins.

3.5. mitoBK_{Ca} interacts with ANT in HEK293T cells

From the potential partners of BK_{Ca} in Table 1, we next selected ANT (matching peptides TAVAPIE, YFPTQALNFAFK) to substantiate the association of the two proteins by biochemical means. Although the analysis software reported ANT2 as the matching protein, the identified peptides are identical in ANT1, which is the isoform that predominates in heart tissue (Graham et al., 1997; Dorner et al., 1999). ANT is of special interest: in addition to its role in exchanging ADP/ATP across the inner mitochondrial membrane, ANT serves as regulator of the mPTP (Morciano et al., 2015; Halestrap and Richardson, 2015). Moreover, its potential association with mitoBK_{Ca} offers a molecular link between regulatory components of the mPTP and the role of mitoBK_{Ca} in the regulation of mPTP (Cheng et al., 2011; Singh et al., 2013).

Figure 5A shows co-immunoprecipitation experiments performed using HEK293T cells co-expressing ANT (c-Myc-DDK tagged) with BK_{Ca} (untagged) and BK_{Ca}-DEC (HA tagged) (lanes 4 and 5) or expressing ANT, BK_{Ca}-DEC or BK_{Ca} alone (lanes 1-3). In these experiments, we immunoprecipitated BK_{Ca} and tested the blots for BK_{Ca} as control (Fig. 5A, top panel) and for co-immunoprecipitated ANT (Fig. 5A, lower panel). Signals of co-immunoprecipitated ANT (squares, lanes 4 and 5) were only present when both ANT and BK_{Ca} (or BK_{Ca}-DEC) were co-expressed. Confirming the molecular mass of ANT, its

immunoprecipitation yielded products with similar molecular mass (not shown). For reverse co-immunoprecipitation see Fig. 7 (lane 13). Fig. 5B demonstrates proper expression of all clones in the input lysates. Note that although expression of BK_{Ca}-DEC was lower in the input lysate (Fig. 5B, upper panel, lanes 2 and 4), its immunoprecipitation was quite efficient yielding bands as intense as those for BK_{Ca} (Fig. 5A, top panel). The co-immunoprecipitation efficiency, calculated as in Fig. 2E, demonstrates that the DEC sequence in BK_{Ca}-DEC enhances the ability of ANT to associate with BK_{Ca} by ~30% (from 0.69±0.02 to 1, n=3). This result is in contrast to Tom22, which interacted equally well with both BK_{Ca} and BK_{Ca}-DEC.

3.6. mitoBK_{Ca} and ANT are imported into mitochondria of HEK293T cells

Next, we investigated the subcellular localization of BK_{Ca} (or BK_{Ca}-DEC) and ANT co-expressed in HEK293T cells using cell fractionation and double-labeled immunoblots. Figure 6 illustrates the distribution of BK_{Ca} (A) and BK_{Ca}-DEC (B) when co-expressed with ANT. Bands around ~135 kDa correspond to BK_{Ca} (A), at ~140 kDa correspond to BK_{Ca}-DEC (B) and bands at ~32 kDa correspond to ANT (A,B). In contrast to Tom22 that distributed along all fractions (Fig. 3), ANT showed a clear-cut enrichment in the “crude” and purified mitochondrial fractions indicating that at the time of cell harvesting the vast majority, if not all, synthesized ANT had reached its mitochondrial destination. In line with this view, no signals were detected in the “crude” membrane or cytosolic fractions (within the resolution of our immunoblots). On the other hand, BK_{Ca} and BK_{Ca}-DEC followed the same expression trend as when co-expressed with Tom22 (Fig. 3) with both BK_{Ca} and BK_{Ca}-DEC concentrated in the “crude” mitochondrial fraction but still detected in the purified mitochondrial fraction.

The mean relative abundance of each protein in the different fractions with respect to cell lysates (set to 1) is shown in Fig. 6C-E. Mean values for BK_{Ca} (C) and BK_{Ca}-DEC (D) in “crude” mitochondria fractions were: BK_{Ca}=1.96±0.002 and BK_{Ca}-DEC=1.68±0.10 (n=3 each), and in the purified mitochondria fraction were: BK_{Ca}=0.56±0.10 and BK_{Ca}-DEC=0.31±0.10 (n=3 each). In contrast, the distribution in the “crude” membrane and cytosolic fractions were minimal with the exception of BK_{Ca}-DEC in “crude” membranes (“crude” membranes: BK_{Ca}=0.23±0.10, BK_{Ca}-DEC=0.57±0.10; cytosol: BK_{Ca}=0.06±0.03, BK_{Ca}-DEC=0.02±0.03; n=3 each). ANT mean relative abundance values (E) demonstrated a vast enrichment (32 times) in the purified mitochondrial fraction and a robust segregation in the “crude” mitochondria fraction (10 times) with respect to cell lysates. Mean values were: 32.05±0.99 and 9.70±3.20 (n=3 each), respectively. These results are consistent with the fact that ANT is the most abundant protein in the inner mitochondrial membrane (Liu and Chen, 2013) and validate the cell fractionation protocol used here. Moreover, they indicate that the association between ANT and BK_{Ca} must occur in mitochondria.

3.7. ANT interacts with BK_{Ca} through the channel transmembrane domain

Figure 5C showed that the presence of the DEC sequence can facilitate, but does not determine, the interaction between BK_{Ca} and ANT. Thus, other regions in BK_{Ca} must be of relevance for the association between the two molecules. To address this point, we performed coimmunoprecipitation experiments to define the major region(s) in BK_{Ca}

involved in its association with ANT. The same deletion constructs as in Fig. 4C that lack DEC insert were co-expressed or not (control) with ANT in HEK293T cells. Figure 7A shows an example of a coimmunoprecipitation experiment using anti-DDK mAb to immunoprecipitate ANT and anti-c-Myc pAb to detect immunoprecipitated ANT and co-immunoprecipitated BK_{Ca} proteins in the same blot. Lanes 8-13 show the co-immunoprecipitated BK_{Ca} constructs together with the immunoprecipitated ANT; lanes 1-6 show the corresponding background signals in the absence of ANT expression and lane 7 shows expression of ANT alone.

Signals of 1-343, 1-441, and 1-711 were strong (lanes 8-10, squares), whereas, the C-terminus (322-1113) and "tail" (679-1113) signals were low (lanes 11-12, squares). As reference, lane 13 shows the co-immunoprecipitation of wild type BK_{Ca}. Note that the coimmunoprecipitated BK_{Ca} signals (squares) are much stronger than the corresponding background signals (dashed squares). The immunoblot of corresponding input lysates is shown in Fig. 7B. After subtraction of background signals, the co-immunoprecipitation signals of BK_{Ca} constructs were normalized to the corresponding ANT signals in the immunoprecipitates and to the BK_{Ca} signals in the input lysates to obtain the Co-IP efficiency compared to wild-type BK_{Ca}. Compared to wild-type BK_{Ca}, the Co-IP efficiency was higher for constructs 1-343 and 1-441 (1-343=2.05±0.69; 1-441=1.65±0.34; n=3 each). Protein 1-711 showed very similar ability to interact with ANT (0.91±0.20, n=3 each) compared to the full length BK_{Ca}; whereas, the C-terminus 322-1113 (0.17±0.05, n=3 each) and "tail" 679-1113 (0.33±0.03, n=3 each) had a marked decrease in their ability to associate with ANT. Overall, the results indicate that in HEK293T cells the interaction between BK_{Ca} and ANT is mainly through the transmembrane domain of BK_{Ca} (1-343) and that the whole C-terminus and not only the "tail" as for Tom22 exerts an inhibitory effect in the interaction.

4. Discussion

4.1. Cardiac BK_{Ca} mitochondrial interactome: physiological relevance

This study is the first to address the potential interactome of BK_{Ca} channels specifically in mitochondria, in particular of cardiac mitochondria. In total, we identified 151 mitochondrial proteins that can interact with BK_{Ca}. These partner proteins are involved in 13 physiological mitochondrial functions, including oxidative phosphorylation, TCA cycle, import, and metabolism (Fig. 1 and Table 1). We focused on the heart because mitoBK_{Ca} has a proven physiological role in this organ, acting as a shield from ischemia and reperfusion injury (Xu et al., 2002; Singh et al., 2013; Soltysinska et al., 2014; Balderas et al., 2015), while its activity improves basal mitochondrial respiratory performance (Aon et al., 2010). Moreover, in astrocytoma cells mitoBK_{Ca} electrical activity is influenced by substrates of oxidative phosphorylation (Bednarczyk et al., 2013). Consistent with these functional studies, we found mitochondrial BK_{Ca} partner proteins belonging to four complexes (complex I, III, IV, and V) of the respiratory chain including ATP synthase, cytochrome *c* oxidase and NADH dehydrogenase. Interestingly, in our previous whole brain proteomic studies, we also found these respiratory chain proteins forming part of the BK_{Ca} interactome (Singh et al., 2016). It is worth mentioning that cytochrome *c* oxidase subunit 1 directly binds to the regulatory β1 subunit of BK_{Ca} channel in cardiac cells (Ohya et al., 2005). Because BK_{Ca} was found here

to also be a potential partner of this subunit of cytochrome *c* oxidase (Table 1), it is possible that mitoBK$_{Ca}$ can form a tripartite complex with these subunits in the heart.

mitoBK$_{Ca}$ also participates in the regulation of the mPTP. Inhibition of its activity either by gene silencing in ischemia-reperfusion experiments (Singh et al., 2013) or by pharmacological inhibition under basal conditions (Cheng et al., 2011) promotes the opening of mPTP. The current view on mPTP molecular composition supports ATP synthase dimers or ATP subunit *c* as the core of mPTP surrounded by several regulatory subunits that include ANT (Giorgio et al., 2013; Halestrap and Richardson, 2015; Morciano et al., 2015; Izzo et al., 2016). That ATP synthase and ANT form a supercomplex (ATP synthasome) together with the inorganic phosphate carrier (PiC) is well established (Chen et al., 2004), although in rat cardiac mitochondria ANT can also be observed independently of ATP synthase (Nuskova et al., 2015). The proteomic data yielded several ATP synthase subunits as candidate partners of BK$_{Ca}$ as well as ANT and PiC. This novel information sets the background for future studies to learn whether BK$_{Ca}$ forms part of a megacomplex with the ATP synthase. As a first step, in this work, we chose to study the association of BK$_{Ca}$ with ANT (Figs. 5-7) (see below).

mitoBK$_{Ca}$ is a nuclear-encoded protein and thus, must be imported into mitochondria to fulfill its multiple functions. As will be discussed below, our data also gives initial clues about the mechanisms that could support mitoBK$_{Ca}$ import.

4.2. Tom22, a potential mitochondrial import mechanism for BK$_{Ca}$ channel

A total of 8 proteins of the mitochondrial import system were found as potential partners of BK$_{Ca}$ (Table 1). Specifically, we found the receptor proteins Tom22 and Tom70, and the protein-conducting channel Tom40 of the outer membrane TOM complex (Wenz et al., 2015); and Tim23, Tim16, GrpE1, and MPPA of the inner membrane Tim23-PAM classical presequence import pathway (Schulz et al., 2015). Although BK$_{Ca}$ lacks a presequence, there is precedence in the literature for atypical proteins (e.g. phosphate carrier) that only contain C-terminal or internal targeting sequences, like BK$_{Ca}$, that utilize the Tim23-PAM pathway (Schulz et al., 2015). Thus, BK$_{Ca}$ may be another example of this type of unconventional precursor proteins.

In this work, we scrutinized the association of the receptor protein Tom22 with BK$_{Ca}$ and BK$_{Ca}$-DEC. As mentioned before, the C-terminal DEC splice insert favors BK$_{Ca}$ expression in mitochondria of adult cardiomyocytes making it a candidate for an import signal. Interestingly, both BK$_{Ca}$ isoforms (with or without DEC) associated equally well with Tom22 (Fig. 2). Several explanations are possible: i) that the DEC insert is not essential for the association with Tom22 and that other regions in BK$_{Ca}$ are relevant, ii) that the DEC insert is substrate of another component of the import pathway, or iii) that BK$_{Ca}$ utilizes different import mechanisms depending on the cell type.

Our results also show that both BK$_{Ca}$ isoforms coexist with Tom22 in the “crude” and purified mitochondrial fractions (Fig. 3) demonstrating that both isoforms are able to be imported into mitochondria, and supporting the idea that their association can occur in this organelle. In co-expressing HEK293T cells, BK$_{Ca}$ isoforms were also present in the “crude”

membrane fraction; this is expected as BK_{Ca} can have multiple subcellular locations including the plasma membrane. Tom22 abundance in the cytosolic fraction (likely containing ribosomes) may be an indication of its synthesis at the time of cell harvesting in these cells, but the detection in "crude" membranes is at present enigmatic (Fig. 3E). Previous studies in expressing HeLa cells have shown faint signals in these fractions (Nakamura et al., 2004). The distribution of Tom22 is in clear contrast with the sharp enrichment of ANT in mitochondrial fractions (Fig. 6) arguing against a deficiency in the fractionation protocol or a misstargeting effect due to overexpression. In any event, the results demonstrate beyond doubt that BK_{Ca} can associate with Tom22 via its transmembrane segment and in doing so does not require the presence of the C-terminal DEC insert (Fig. 4). The association could be indirect via a yet to be discovered linking partner or direct protein-protein interaction between the two molecules. A simple picture in BK_{Ca} import route based on these results and proteomic data can include the recognition of BK_{Ca} precursor protein by Tom22 and translocation via Tom40 to reach the inner mitochondrial membrane (Fig. 8) perhaps driven by the Tim23-PAM complex. At present, we can not exclude the possibility that BK_{Ca} association with Tom22 could serve another function independent of its import. In fact, new non-assembled intermediate complexes have been recently discovered by proteomics between components of the Tom system (Tom40 and Tom22) and Porin 1 (the voltage dependent anion channel homolog in yeast) (Muller et al., 2016).

4.3. BK_{Ca} interaction with ANT

We have demonstrated the novel interaction between ANT and BK_{Ca} in co-expressing HEK293T cells (Figs. 5 and 7). As for Tom22, both BK_{Ca} isoforms (with and without DEC) could associate with ANT; however, the presence of DEC sequence improved their association. The trend in subcellular distribution of BK_{Ca} (with or without DEC) co-expressed with ANT including the relative abundance in the purified mitochondria fraction was similar to that observed with Tom22 (Figs. 3 and 6) indicating that its distribution to mitochondria was not biased by the co-expressed partner. At the time of harvesting of the cells, ANT was dramatically enriched in the purified mitochondria fraction and BK_{Ca} though concentrated in the "crude" mitochondria fraction was also present in purified mitochondria (Fig. 6). Because ANT was so enriched in the purified mitochondria fraction, the likelihood that the interaction between the two proteins happens in the mitochondria is high. The fact that ANT resides in the inner mitochondrial membrane gives further support to the notion that BK_{Ca} resides in this location as well (Fig. 8) (Xu et al., 2002). The association of BK_{Ca} with ANT in the inner mitochondrial membrane could be in conjunction with the ATP synthasome as mentioned before (Fig. 8) or independent of it. In any case, the interaction of BK_{Ca} and ANT discovered in this work takes place via the transmembrane domain of BK_{Ca} (Fig. 7) either directly with ANT or via an unknown intermediary partner. Together our results open a new window to understand how BK_{Ca} channel regulates the activity of mPTP inasmuch as ANT is a regulator of mPTP (Halestrap and Richardson, 2015). A functional coupling between BK_{Ca} and ANT could be an additional factor in the complex regulation of mPTP.

5. Conclusion

The results from this work demonstrate the novel interactions of BK_{Ca} with Tom22 and ANT, and provide a molecular framework to better understand the intricacies of BK_{Ca} mitochondrial import mechanism and function.

Acknowledgements

This work was supported by the National Institutes of Health [grant HL107418 to LT, ES, RO].

Abbreviations

ANT	adenine nucleotide translocator
BK_{Ca}	large conductance voltage- and Ca^{2+}-dependent K^+ channel
BK_{Ca}-DEC	BK_{Ca} containing DEC splice insert at the C-terminus
co-IP	co-immunoprecipitation
DEC	a 50 amino acid C-terminal BK_{Ca} splice insert
GST	glutathione *S*-transferase
LC/MS/MS	liquid chromatography, mass spectrometry in tandem
mAb	monoclonal antibody
mitoBK_{Ca}	mitochondrial BK_{Ca}
mPTP	mitochondrial permeability transition pore
pAb	polyclonal antibody
Tom22	mitochondrial import receptor subunit Tom22

References

Aon MA, Cortassa S, Wei AC, Grunnet M, O'Rourke B. Energetic performance is improved by specific activation of K+ fluxes through K(Ca) channels in heart mitochondria. Biochim.Biophys.Acta. 2010; 1797:71–80. [PubMed: 19744465]

Balderas E, Zhang J, Stefani E, Toro L. Mitochondrial BKCa channel. Front Physiol. 2015; 6:104. [PubMed: 25873902]

Bednarczyk P, Wieckowski MR, Broszkiewicz M, Skowronek K, Siemen D, Szewczyk A. Putative Structural and Functional Coupling of the Mitochondrial BK Channel to the Respiratory Chain. PLoS.One. 2013; 8:e68125. [PubMed: 23826369]

Chen C, Ko Y, Delannoy M, Ludtke SJ, Chiu W, Pedersen PL. Mitochondrial ATP synthasome: three-dimensional structure by electron microscopy of the ATP synthase in complex formation with carriers for Pi and ADP/ATP. J.Biol.Chem. 2004; 279:31761–31768. [PubMed: 15166242]

Cheng Y, Gulbins E, Siemen D. Activation of the permeability transition pore by Bax via inhibition of the mitochondrial BK channel. Cell Physiol Biochem. 2011; 27:191–200. [PubMed: 21471707]

Dorner A, Olesch M, Giessen S, Pauschinger M, Schultheiss HP. Transcription of the adenine nucleotide translocase isoforms in various types of tissues in the rat. Biochim.Biophys.Acta. 1999; 1417:16–24. [PubMed: 10076031]

Giorgio V, von SS, Antoniel M, Fabbro A, Fogolari F, Forte M, Glick GD, Petronilli V, Zoratti M, Szabo I, Lippe G, Bernardi P. Dimers of mitochondrial ATP synthase form the permeability transition pore. Proc Natl Acad Sci U S A. 2013; 110:5887–5892. [PubMed: 23530243]

Gorini G, Ponomareva O, Shores KS, Person MD, Harris RA, Mayfield RD. Dynamin-1 co-associates with native mouse brain BKCa channels: proteomics analysis of synaptic protein complexes. FEBS Lett. 2010; 584:845–851. [PubMed: 20114047]

Graham BH, Waymire KG, Cottrell B, Trounce IA, MacGregor GR, Wallace DC. A mouse model for mitochondrial myopathy and cardiomyopathy resulting from a deficiency in the heart/muscle isoform of the adenine nucleotide translocator. Nat.Genet. 1997; 16:226–234. [PubMed: 9207786]

Graham JM. Purification of a crude mitochondrial fraction by density-gradient centrifugation. Curr.Protoc.Cell Biol. 2001 Chapter 3, Unit.

Halestrap AP, Richardson AP. The mitochondrial permeability transition: a current perspective on its identity and role in ischaemia/reperfusion injury. J.Mol.Cell Cardiol. 2015; 78:129–141. [PubMed: 25179911]

Izzo V, Bravo-San Pedro JM, Sica V, Kroemer G, Galluzzi L. Mitochondrial Permeability Transition: New Findings and Persisting Uncertainties. Trends Cell Biol. 2016

Kathiresan T, Harvey M, Orchard S, Sakai Y, Sokolowski B. A protein interaction network for the large conductance Ca(2+)-activated K(+) channel in the mouse cochlea. Mol.Cell Proteomics. 2009; 8:1972–1987. [PubMed: 19423573]

Li M, Zhang Z, Koh H, Lu R, Jiang Z, Alioua A, Garcia-Valdes J, Stefani E, Toro L. The beta1-Subunit of the MaxiK Channel Associates with the Thromboxane A2 Receptor and Reduces Thromboxane A2 Functional Effects. J.Biol.Chem. 2013; 288:3668–3677. [PubMed: 23255603]

Liu Y, Chen XJ. Adenine nucleotide translocase, mitochondrial stress, and degenerative cell death. Oxid.Med.Cell Longev. 2013; 2013:146860. [PubMed: 23970947]

Ma D, Nakata T, Zhang G, Hoshi T, Li M, Shikano S. Differential trafficking of carboxyl isoforms of Ca2+-gated (Slo1) potassium channels. FEBS Lett. 2007; 581:1000–1008. [PubMed: 17303127]

Mayer A, Nargang FE, Neupert W, Lill R. MOM22 is a receptor for mitochondrial targeting sequences and cooperates with MOM19. EMBO J. 1995; 14:4204–4211. [PubMed: 7556061]

Meera P, Wallner M, Song M, Toro L. Large conductance voltage- and calcium-dependent K+ channel, a distinct member of voltage-dependent ion channels with seven N-terminal transmembrane segments (S0-S6), an extracellular N terminus, and an intracellular(S9-S10) C terminus. Proc.Natl.Acad.Sci.U.S.A. 1997; 94:14066–14071. [PubMed: 9391153]

Misonou H, Menegola M, Buchwalder L, Park EW, Meredith A, Rhodes KJ, Aldrich RW, Trimmer JS. Immunolocalization of the Ca2+-activated K+ channel Slo1 in axons and nerve terminals of mammalian brain and cultured neurons. J Comp Neurol. 2006; 496:289–302. [PubMed: 16566008]

Morciano G, Giorgi C, Bonora M, Punzetti S, Pavasini R, Wieckowski MR, Campo G, Pinton P. Molecular identity of the mitochondrial permeability transition pore and its role in ischemia-reperfusion injury. J.Mol.Cell Cardiol. 2015; 78:142–153. [PubMed: 25172387]

Muller CS, Bildl W, Haupt A, Ellenrieder L, Becker T, Hunte C, Fakler B, Schulte U. Cryo-slicing Blue Native-Mass Spectrometry (csBN-MS), a Novel Technology for High Resolution Complexome Profiling. Mol.Cell Proteomics. 2016; 15:669–681. [PubMed: 26598645]

Nakamura Y, Suzuki H, Sakaguchi M, Mihara K. Targeting and assembly of rat mitochondrial translocase of outer membrane 22 (TOM22) into the TOM complex. J.Biol.Chem. 2004; 279:21223–21232. [PubMed: 14985332]

Nuskova H, Mracek T, Mikulova T, Vrbacky M, Kovarova N, Kovalcikova J, Pecina P, Houstek J. Mitochondrial ATP synthasome: Expression and structural interaction of its components. Biochem.Biophys.Res.Commun. 2015; 464:787–793. [PubMed: 26168732]

Ohya S, Kuwata Y, Sakamoto K, Muraki K, Imaizumi Y. Cardioprotective effects of estradiol include the activation of large-conductance Ca(2+)-activated K(+) channels in cardiac mitochondria. Am.J.Physiol Heart Circ.Physiol. 2005; 289:H1635–H1642. [PubMed: 16113069]

Schulz C, Schendzielorz A, Rehling P. Unlocking the presequence import pathway. Trends Cell Biol. 2015; 25:265–275. [PubMed: 25542066]

Singh H, Li M, Hall L, Chen S, Sukur S, Lu R, Caputo A, Meredith AL, Stefani E, Toro L. MaxiK channel interactome reveals its interaction with GABA transporter 3 and heat shock protein 60 in the mammalian brain. Neuroscience. 2016; 317:76–107. [PubMed: 26772433]

Singh H, Lu R, Bopassa JC, Meredith AL, Stefani E, Toro L. mitoBKCa is encoded by the Kcnma1 gene, and a splicing sequence defines its mitochondrial location. Proc Natl Acad Sci U S A. 2013; 110:10836–10841. [PubMed: 23754429]

Singh H, Lu R, Rodriguez PF, Wu Y, Bopassa JC, Stefani E, Toro L. Visualization and quantification of cardiac mitochondrial protein clusters with STED microscopy. Mitochondrion. 2012; 12:230–236. [PubMed: 21982778]

Singh H, Warburton S, Vondriska TM, Khakh BS. Proteomics to identify proteins interacting with P2X2 ligand-gated cation channels. J.Vis.Exp. 2009

Sokolowski B, Orchard S, Harvey M, Sridhar S, Sakai Y. Conserved BK channel-protein interactions reveal signals relevant to cell death and survival. PLoS.One. 2011; 6:e28532. [PubMed: 22174833]

Soltysinska E, Bentzen BH, Barthmes M, Hattel H, Thrush AB, Harper ME, Qvortrup K, Larsen FJ, Schiffer TA, Losa-Reyna J, Straubinger J, Kniess A, Thomsen MB, Bruggemann A, Fenske S, Biel M, Ruth P, Wahl-Schott C, Boushel RC, Olesen SP, Lukowski R. KCNMA1 encoded cardiac BK channels afford protection against ischemia reperfusion injury. PLoS.One. 2014; 9:e103402. [PubMed: 25072914]

Toro L, Li M, Zhang Z, Singh H, Wu Y, Stefani E. MaxiK channel and cell signalling. Pflugers Arch. 2013

Wallner M, Meera P, Ottolia M, Kaczorowski GJ, Latorre R, Garcia ML, Stefani E, Toro L. Characterization of and modulation by a beta-subunit of a human maxi KCa channel cloned from myometrium. Receptors.Channels. 1995; 3:185–199. [PubMed: 8821792]

Wenz LS, Opalinski L, Wiedemann N, Becker T. Cooperation of protein machineries in mitochondrial protein sorting. Biochim.Biophys.Acta. 2015; 1853:1119–1129. [PubMed: 25633533]

Xu W, Liu Y, Wang S, McDonald T, Van Eyk JE, Sidor A, O'Rourke B. Cytoprotective role of Ca2+-activated K+ channels in the cardiac inner mitochondrial membrane. Science. 2002; 298:1029–1033. [PubMed: 12411707]

Highlights

- 151 mitochondrial BK_{Ca} channel protein partners are revealed by proteomics
- A molecular framework defining BK_{Ca} mitochondrial protein relationships is provided
- Novel partners of BK_{Ca} are Tom22 import protein and ANT nucleotide translocator
- BK_{Ca} interaction with ANT is enhanced by the 50 amino acid BK_{Ca} splice insert, DEC
- The BK_{Ca} transmembrane domain is required for the interaction with Tom 22 and ANT

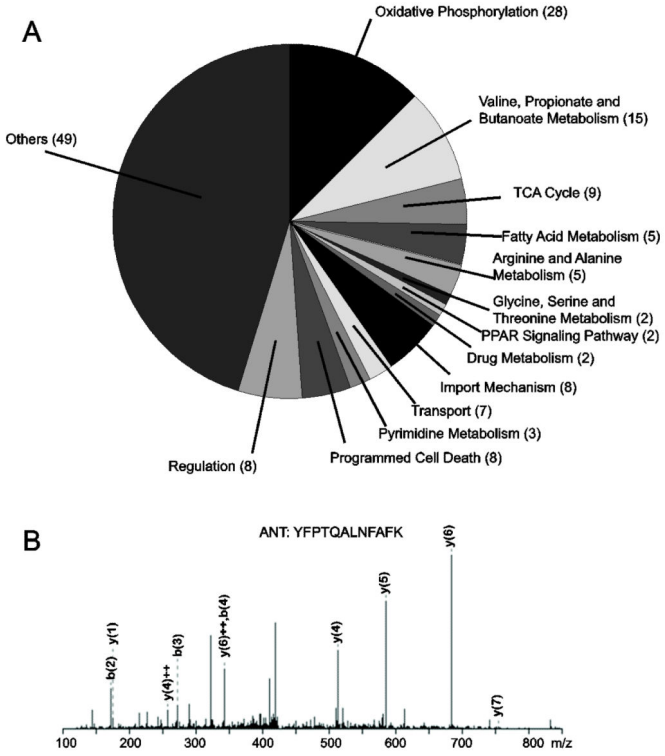

Figure 1. Mitochondrial partners of cardiac mitoBK$_{Ca}$ predict new channel functions

(A) Gene ontology analysis using DAVID of mitochondrial BK$_{Ca}$ proteome revealed mitoBK$_{Ca}$ potential involvement with 13 mitochondrial functions in the heart. Numbers in parenthesis correspond to the number of proteins allocated to each group. “Transport” group was entered manually. Isolation of BK$_{Ca}$ partners was performed using pull-down and immunoprecipitation with: 1) Recombinant GST-DEC and mitochondrial lysates of isolated cardiomyocytes, 2) Recombinant GST-DEC and whole-cardiomyocyte lysates, and 3) Monoclonal anti-BK$_{Ca}$ antibody and lysates of Percoll-purified mitochondria from left ventricle. Controls included GST pull-down and IgG immunoprecipitation (see Methods). A total of 151 mitochondrial proteins with a score>21 were identified. (B) Example of mass spectrum of a peptide matching ANT.

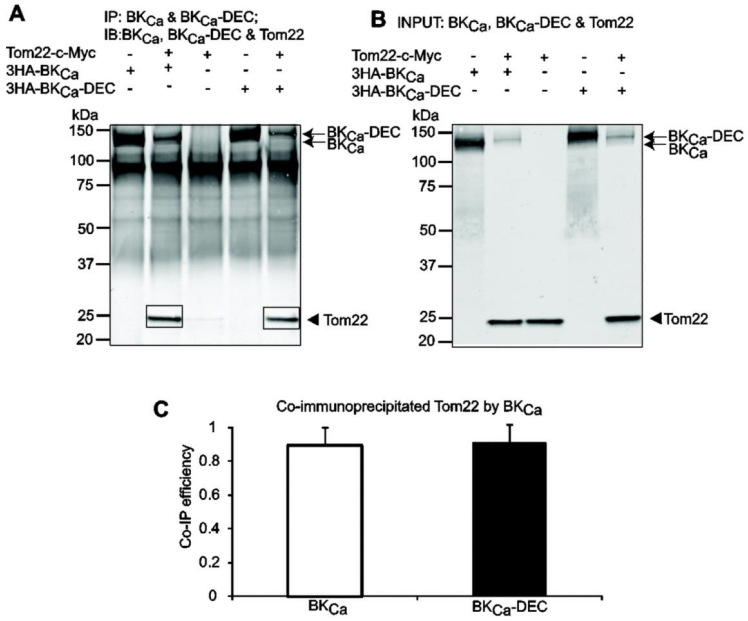

Figure 2. BK_{Ca} interacts with Tom22 in HEK293T cells

Cells were co-transfected with BK_{Ca}, BK_{Ca}-DEC and Tom22 in different combinations (+, present; -, absent). Co-immunoprecipitated products are highlighted with squares. (A) Immunoblot demonstrating that BK_{Ca} and BK_{Ca}-DEC pull down Tom22. BK_{Ca} constructs were immunoprecipitated with anti-HA pAb and detected with anti-HA mAb (arrows) and co-immunoprecipitated Tom22 was detected with anti-c-Myc mAb (arrowhead, squares). Primary antibodies were incubated at the same time. (B) Immunoblot showing proper expression of BK_{Ca} constructs (arrows) and Tom22 (arrowhead) in the input lysates. (C) BK_{Ca} and BK_{Ca}-DEC efficiency in pulling down Tom22 is similar (n=3 each). Co-IP efficiency was determined by first subtracting background signals, which in this case were negligible, and calculating the ratio of the band intensities of co-immunoprecipitated Tom22 (i.e. A, squares) to corresponding immunoprecipitated BK_{Ca} constructs (i.e.. A, arrows), and normalized to Tom22 intensity in the corresponding input lysates (i.e. B, arrowhead). In this and following figures, image analysis was performed with MetaMorph Image Analysis Software (Molecular Devices).

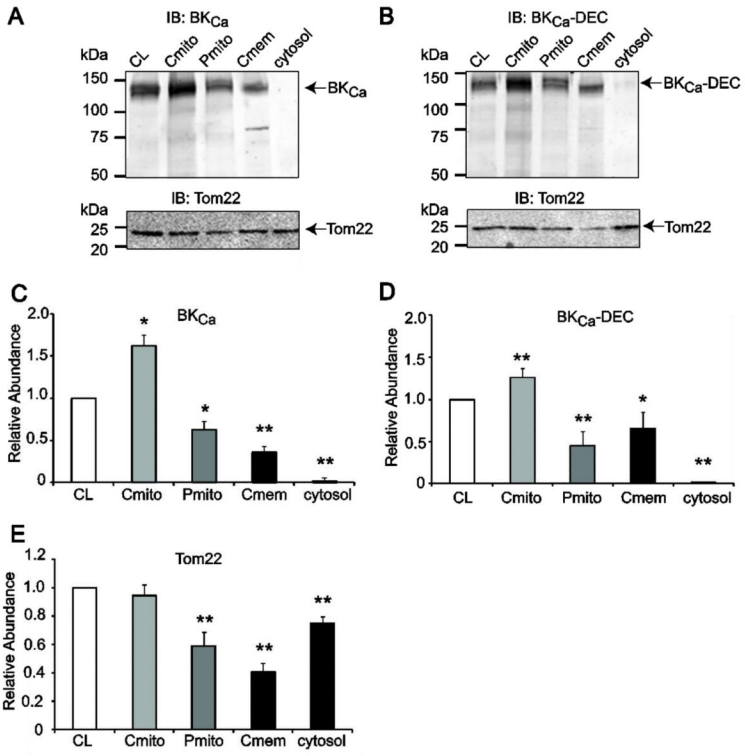

Figure 3. BK_{Ca} and Tom22 are imported into mitochondria in HEK293T cells

(A and B) Dually labeled immunoblots of BK_{Ca} (A, top) or BK_{Ca}-DEC (B, top) co-expressed with Tom22 (bottom) in different cellular fractions: CL, whole cell lysate; Cmito, "crude" mitochondria; Pmito, Percoll-purified mitochondria; Cmem, "crude" membranes; cytosol, cytosolic fraction. BK_{Ca} and Tom22 images were separated for clarity. In panel (A), BK_{Ca} and Tom22 blots are from different experiments. BK_{Ca} constructs were recognized with anti-HA mAb (upper panels); Tom22 was recognized with anti-c-Myc pAb (lower panels). (C-E) Mean values of BK_{Ca}, BK_{Ca}-DEC and Tom22 relative abundance in different cellular fractions show that BK_{Ca}, BK_{Ca}-DEC and Tom22 were imported into "crude" and purified mitochondrial fractions, though not enriched. Values for Tom22 were pooled from both BK_{Ca} and BK_{Ca}-DEC experiments. *, $p<0.05$ compared to CL. **, $p<0.01$ compared to CL. n=3 independent experiments.

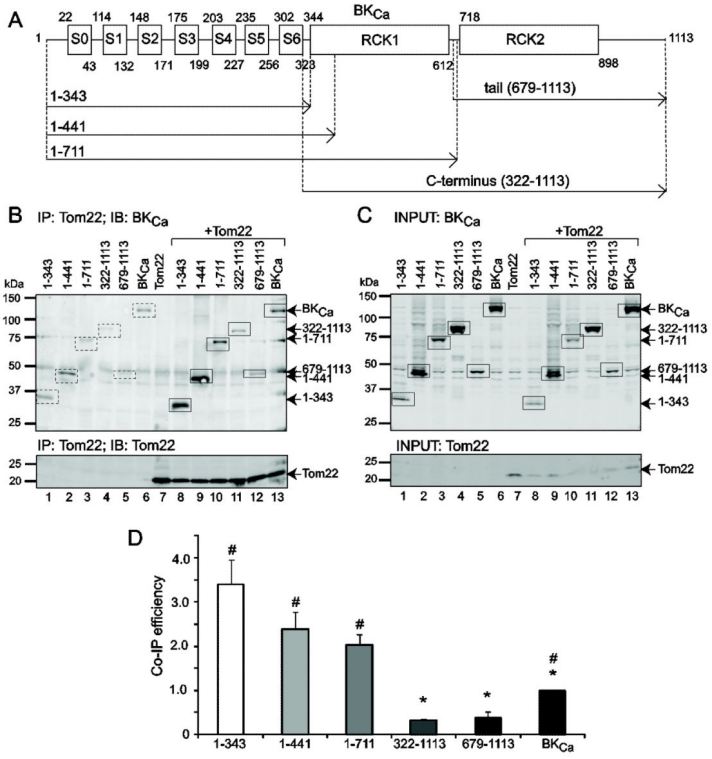

Figure 4. BK_{Ca} channel transmembrane region interacts with Tom22

(A) Scheme of wild type BK_{Ca} (1-1113) pore-forming α-subunit and different truncated proteins that were either expressed alone or co-expressed with Tom22. Numbers correspond to amino acid numbers in NCBI Accession No. U11058.2. S0-S6, transmembrane regions form the channel voltage sensor. Linker between S5-S6 forms the tetrameric channel pore region. Regulator of potassium conductance (RCK) 1 and 2 are Ca^{2+} sensors. (B) Dually labeled immunoblot for BK_{Ca} (top) and Tom22 (bottom) showing the ability of Tom22 to co-immunoprecipitate different BK_{Ca} channel regions (lanes 8-13, top). BK_{Ca} and Tom22 images were separated for clarity. Lanes 1-7 are controls expressing BK_{Ca} constructs or Tom22 alone. Squares and arrows mark the expected band sizes of each construct. Background signals (dashed squares, lanes 1-7, top) were much lower than the signals of the co-immunoprecipitated BK_{Ca} products (squares, lanes 8-13, top) and were subtracted to calculate Co-IP efficiency in (D). As control, the lower panel shows Tom22 successful immunoprecipitation. Tom22 was immunoprecipitated with anti-DDK mAb. Co-immunoprecipitated BK_{Ca} proteins were detected with anti-c-Myc pAb, and Tom22 was detected with anti-DDK mAb. (C) Control immunoblot of input lysates of cells expressing different BK_{Ca} regions (upper panel) and Tom22 (lower panel). BK_{Ca} constructs were detected with anti-c-Myc pAb and Tom22 was detected with anti-DDK mAb. Squares and arrows mark the expected band sizes. (D) Tom22 efficiency in pulling down different BK_{Ca} regions indicates that BK_{Ca} channel interacts with Tom22 mainly through the transmembrane domain (construct 1-343). Co-IP efficiency was calculated after subtracting background signals and calculating the ratio of the band intensities of co-immunoprecipitated BK_{Ca} constructs (i.e. B, top, lanes 8-13, squares) to corresponding immunoprecipitated Tom22 (i.e. B, lower panel, lanes 8-13), and normalized to BK_{Ca}

construct intensities in the corresponding input lysates (i.e.. C, top, lanes 8-13). *, $p<0.05$ with respect to construct 1-343; #, $p<0.05$ with respect to the C-terminus (322-1113).

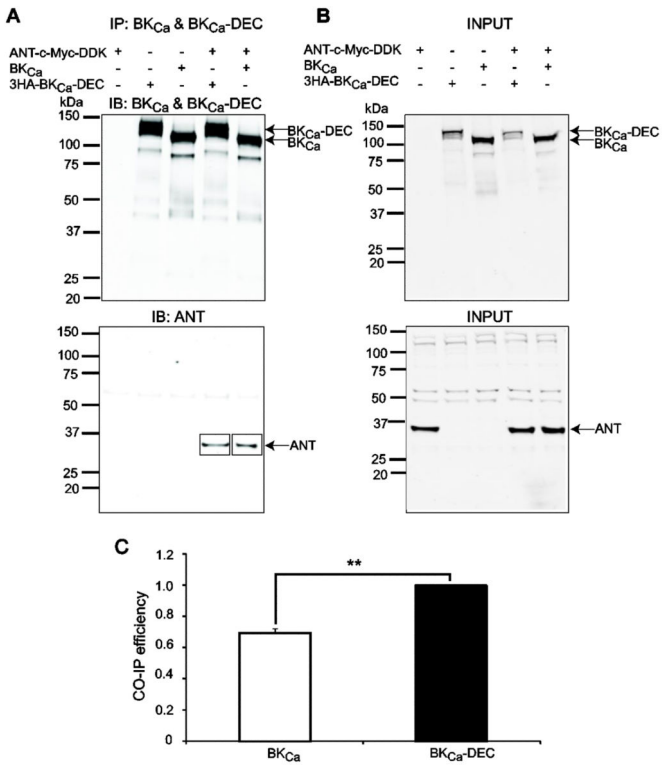

Figure 5. BK_{Ca} interacts with ANT in HEK293T cells

Cells were co-transfected with BK_{Ca}, BK_{Ca}-DEC and ANT in different combinations (+, present; -, absent). (A) BK_{Ca} and BK_{Ca}-DEC were immunoprecipitated with anti-BK_{Ca} mAb and detected with anti-BK_{Ca} pAb (top panel); coimmunoprecipitated ANT was detected with anti-Flag pAb that recognizes the DDK epitope (lower panel, squares). Top and bottom panels are different blots using the same immunoprecipitation products. (B) Input lysates showing proper expression of BK_{Ca} (top panel) and ANT (lower panel). BK_{Ca} and BK_{Ca}-DEC were detected with anti-BK_{Ca} pAb and ANT was detected with anti-Flag pAb. (C) Mean values of BK_{Ca} and BK_{Ca}-DEC efficiency in pulling down ANT show that BK_{Ca}-DEC associates better with ANT by about 30%. Co-immunoprecipitation efficiency was calculated as described in the legend to Figure 2 for Tom22. **, $p<0.01$, n=3 independent experiments.

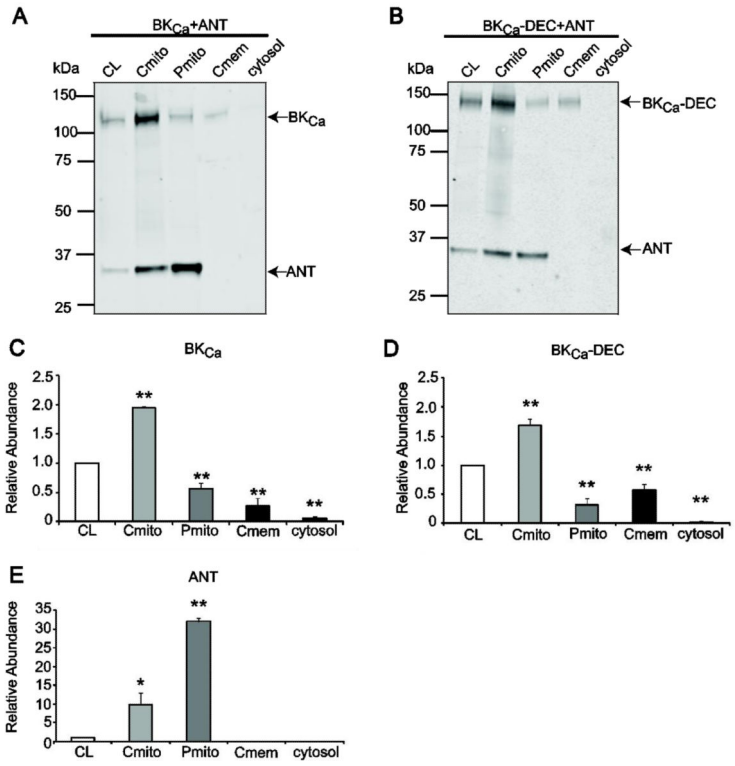

Figure 6. BK_{Ca} and ANT are imported into mitochondria of HEK293T cells

A and B, Dually labeled immunoblots of BK_{Ca} (A) or BK_{Ca}-DEC (B) co-expressed with ANT show that the three constructs were imported into "crude" and purified mitochondria fractions. Note the enrichment of ANT in the purified mitochondria fraction. Labels are as in Fig. 3. BK_{Ca} was recognized with anti-HA mAb. ANT was recognized with anti-c-Myc pAb. C, D, and E, Quantification of BK_{Ca}, BK_{Ca}-DEC and ANT relative abundance in different cellular fractions. *, $p<0.05$ compared to CL; **, $p<0.01$compared to CL. n=3 independent experiments.

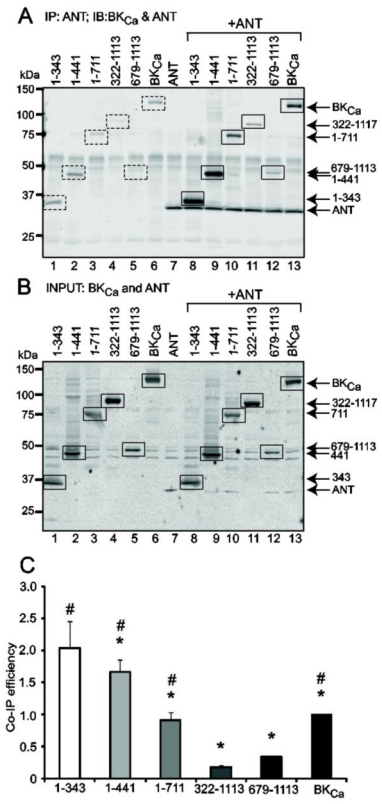

Figure 7. Molecular determinant of BK_{Ca} channel interaction with ANT

Different regions of BK_{Ca} and wild-type BK_{Ca} (see scheme in Fig. 4A) were either expressed alone or co-expressed with ANT. (A) Dually labeled immunoblot shows that immunoprecipitated ANT pulled down wild-type and deletion BK_{Ca} constructs (lanes 8-13) to different degrees. Squares and arrows mark the bands of the expected sizes. Dashed squares mark background signals, which were subtracted for the analysis in (C). ANT was immunoprecipitated with anti-DDK mAb. Coimmunoprecipitated BK_{Ca} proteins and ANT were detected with anti-c-Myc pAb. (B) Control immunoblot of input lysates of cells expressing different BK_{Ca} regions and ANT. (C) ANT efficiency in pulling different BK_{Ca} constructs indicates that BK_{Ca} channel interacts with ANT mainly through the transmembrane domain (construct 1-343). *, $p<0.05$ with respect to construct 1-343; #, $p<0.05$ with respect to construct 322-1113. n=3 independent experiments.

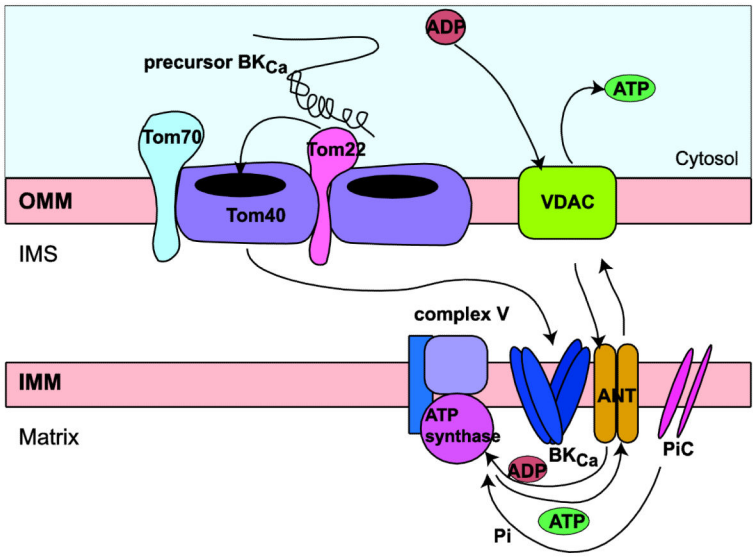

Figure 8. Scheme of potential mitoBK$_{Ca}$ mport route and interactions in mitochondria

Overall the results suggest that the precursor BK$_{Ca}$ could be recognized by Tom22 in the outer mitochondrial membrane (OMM) and imported by Tom 40 to reach its final destination in the inner mitochondrial membrane (IMM). At the IMM, mitoBK$_{Ca}$ interacts with ADP/ATP translocase (ANT). The interaction could be independent or in combination with known partners of ANT, e.g. the synthasome (ATP synthase and the phosphate carrier, PiC), and implies a new role of mitoBK$_{Ca}$ in mitochondrial metabolism. Of note, proteomic analysis (Table 1) points to the possibility that BK$_{Ca}$ may also interact with the voltage-dependent anion channel VDAC, the ATP synthase and PiC. VDAC, allows ATP/ADP exchange with the intracellular milieu. IMS, intermembrane space.

Table 1

BK_{Ca} channel-interacting mitochondrial proteins identified by LC/MS/MS

Proteins	Uniprot ID	Mass, Da	Score	Peptides
Oxidative Phosphorylation				
NADH-ubiquinone oxidoreductase 75 kDa subunit (*C,B*)	NDUS1_RAT	80331	785	18
ATP synthase protein 8 *(B)*	ATP8_RAT	7637	514	4
Succinate dehydrogenase [ubiquinone] flavoprotein subunit *(C)*	DHSA_RAT	72596	501	10
NADH dehydrogenase [ubiquinone] iron-sulfur protein 2 *(C)*	NDUS2_RAT	52927	268	8
Cytochrome c oxidase subunit 4 isoform 1 *(C)*	COX41_RAT	19559	266	10
ATP synthase-coupling factor 6 *(B)*	ATP5J_RAT	12487	236	3
NADH dehydrogenase [ubiquinone] flavoprotein 2 *(B)*	NDUV2_RAT	27703	140	3
NADH dehydrogenase [ubiquinone] iron-sulfur protein 4 (*A,B*)	NDUS4_RAT	19785	135	4
Cytochrome b-c1 complex subunit Rieske *(B)*	UCRI_RAT	29712	128	7
NADH dehydrogenase [ubiquinone] 1 alpha subcomplex subunit 10 *(C)*	NDUAA_RAT	40753	127	5
ATP synthase subunit e *(B)*	ATP5I_RAT	8249	121	2
Cytochrome c oxidase subunit 7A2 (*A,B,C*)	CX7A2_RAT	9347	95	1
Succinate dehydrogenase [ubiquinone] iron-sulfur subunit *(A)*	DHSB_RAT	32607	95	3
Cytochrome c oxidase subunit 6C-2 *(B)*	CX6C2_RAT	8449	93	4
NADH dehydrogenase [ubiquinone] 1 alpha subcomplex subunit 11 *(C)*	NDUAB_RAT	15129	73	2
NADH dehydrogenase [ubiquinone] flavoprotein 3 (*B,C*)	NDUV3_RAT	11934	72	3
ATP synthase subunit epsilon *(B)*	ATP5E_RAT	5820	46	1
ATP synthase subunit d, mitochondrial (*A, C*)	ATP5H_RAT	18809	44	2
Cytochrome c oxidase subunit 1 *(B)*	COX1_RAT	56956	40	3
ATP synthase subunit a (*(B), (C)*)	ATP6_RAT	25034	38	1
Cytochrome c oxidase subunit 6A2 *(B)*	CX6A2_RAT	10594	30	1
Cytochrome b-c1 complex subunit 8 *(B)*	QCR8_RAT	9843	29	3
ATP synthase lipid-binding protein *(C)*	AT5G1_RAT	14463	29	2
NADH dehydrogenase [ubiquinone] iron-sulfur protein 6 *(B)*	NDUS6_RAT	12946	27	3
NADH dehydrogenase [ubiquinone] 1 alpha subcomplex assembly factor 4 *(C)*	NDUF4_RAT	20146	27	4
Cytochrome c oxidase subunit 6C-1 *(C)*	CX6C1_RAT	8547	26	1
ATP synthase subunit s *(C)*	ATP5S_RAT	23765	25	1
NADH-ubiquinone oxidoreductase chain 4 *(C)*	NU4M_RAT	51937	21	2
Valine, Propionate and Butanoate Metabolism				
Trifunctional enzyme subunit alpha *(A)*	ECHA_RAT	83297	796	20

Proteins	Uniprot ID	Mass, Da	Score	Peptides
3-hydroxyacyl-CoA dehydrogenase type-2 *(A)*	HCD2_RAT	27343	125	4
Short-chain specific acyl-CoA dehydrogenase *(A)*	ACADS_RAT	45022	87	1
Malonyl-CoA decarboxylase *(C)*	DCMC_RAT	55298	81	5
Isovaleryl-CoA dehydrogenase *(C)*	IVD_RAT	46862	64	2
2-Oxoisovalerate dehydrogenase subunit alpha (*B, C*)	ODBA_RAT	50418	50	2
Methylcrotonoyl-CoA carboxylase beta chain (*A, C*)	MCCB_RAT	61992	43	2
Acyl-coenzyme A synthetase ACSM2 *(A)*	ACSM2_RAT	64617	41	3
Propionyl-CoA carboxylase beta chain *(C)*	PCCB_RAT	59216	38	2
Methylcrotonoyl-CoA carboxylase subunit alpha (*A, B, C*)	MCCA_RAT	79564	25	2
3-Hydroxyisobutyrate dehydrogenase *(A)*	3HIDH_RAT	35679	24	2
3-Hydroxyisobutyrate dehydrogenase *(A)*	3HIDH_RAT	35679	24	2
Succinate-semialdehyde dehydrogenase *(B)*	SSDH_RAT	56723	23	1
Propionyl-CoA carboxylase alpha chain (*A, C*)	PCCA_RAT	82198	23	5
Dihydrolipoyl dehydrogenase *(B)*	DLDH_RAT	54574	22	3
TCA Cycle				
Pyruvate dehydrogenase E1 component subunit alpha, somatic form *(A)*	ODPA_RAT	43883	448	9
Malate dehydrogenase *(B)*	MDHM_RAT	36117	161	7
Succinyl-CoA ligase [GDP-forming] subunit alpha *(B)*	SUCA_RAT	36524	134	5
Dihydrolipoyllysine-residue acetyltransferase component of pyruvate dehydrogenase complex *(C)*	ODP2_RAT	67637	127	6
Fumarate hydratase *(A)*	FUMH_RAT	54714	126	8
Isocitrate dehydrogenase [NAD] subunit beta*(A)*	IDH3B_RAT	42612	125	10
[Pyruvate dehydrogenase [lipoamide]] kinase isozyme 2 *(B)*	PDK2_RAT	46304	105	7
[Pyruvate dehydrogenase [lipoamide]] kinase isozyme 1 *(A)*	PDK1_RAT	49392	88	6
Isocitrate dehydrogenase [NAD] subunit gamma 1 *(A)*	IDHG1_RAT	43223	34	3
Fatty Acid Metabolism				
Very long-chain specific acyl-CoA dehydrogenase *(C)*	ACADV_RAT	71047	801	16
Carnitine O-palmitoyltransferase 1 (*A, B*)	CPT1B_RAT	89129	701	13
Carnitine O-palmitoyltransferase 2 (*A, C*)	CPT2_RAT	74634	210	7
Long-chain-fatty-acid--CoA ligase 6 (*A, B*)	ACSL6_RAT	79156	52	4
Peroxisomal 3,2-trans-enoyl-CoA isomerase *(A)*	PECI_RAT	43336	50	3
Arginine and Alanine Metabolism				
Glutamate dehydrogenase 1 *(C)*	DHE3_RAT	61719	190	12
Amine oxidase [flavin-containing] A (*A, C*)	AOFA_RAT	60097	111	4
Delta-1-pyrroline-5-carboxylate dehydrogenase *(B)*	AL4A1_RAT	62286	86	4

Proteins	Uniprot ID	Mass, Da	Score	Peptides
Carbamoyl-phosphate synthase *(C)*	CPSM_RAT	165673	25	7
Amine oxidase [flavin-containing] B *(B)*	AOFB_RAT	59049	24	2
Glycine, Serine and Threonine Metabolism				
5-Aminolevulinate synthase, nonspecific *(B)*	HEM1_RAT	71830	28	5
Sarcosine dehydrogenase *(A)*	SARDH_RAT	102573	21	2
PPAR Signaling Pathway				
Glycerol kinase *(A)*	GLPK_RAT	58238	37	2
Sterol 26-hydroxylase *(C)*	CP27A_RAT	60980	30	3
Drug Metabolism				
Glutathione S-transferase P *(A)*	GSTP1_RAT	23652	80	2
Glutathione S-transferase kappa 1 *(A)*	GSTK1_RAT	25590	27	2
Import Mechanism				
Sorting and assembly machinery component 50 homolog *(C)*	SAM50_RAT	52384	372	12
GrpE protein homolog 1 (*B, D*)	GRPE1_RAT	24510	303	9
Mitochondrial-processing peptidase subunit alpha *(C)*	MPPA_RAT	59083	165	7
Mitochondrial import inner membrane translocase subunit TIM16 *(C)*	TIM16_RAT	13722	103	1
Mitochondrial import receptor subunit TOM22 *(B)*	TOM22_RAT	15481	94	1
Mitochondrial import inner membrane translocase subunit Tim23 *(C)*	TIM23_RAT	22064	45	2
Mitochondrial import receptor subunit TOM40 *(A)*	TOM40_RAT	38294	35	2
Mitochondrial import receptor subunit TOM70 *(A)*	TOM70_RAT	68143	24	2
Transport (Channels and Carriers)*				
Voltage-dependent anion-selective channel protein 1 (*A, C*)	VDAC1_RAT	30851	173	4
Phosphate carrier protein *(C)*	MPCP_RAT	39876	50	2
ADP/ATP translocase 2 (*(B),E*)	ADT2_RAT	33108	43	2
ATP-binding cassette sub-family B member 7 *(C)*	ABCB7_RAT	82848	40	6
Voltage-dependent anion-selective channel protein 3 *(C)*	VDAC3_RAT	31178	32	2
Tricarboxylate transport protein *(B)*	TXTP_RAT	34156	24	4
Calcium-binding mitochondrial carrier protein SCaMC-2 *(C)*	SCMC2_RAT	53060	24	1
Pyrimidine Metabolism				
GTP:AMP phosphotransferase *(C)*	KAD3_RAT	25479	98	3
Thymidylate synthase *(A)*	TYSY_RAT	35280	30	2
Thioredoxin reductase 2 *(A)*	TRXR2_RAT	57167	23	4
Programmed Cell Death				

Proteins	Uniprot ID	Mass, Da	Score	Peptides
Apoptosis-inducing factor 1 *(C)*	AIFM1_RAT	66966	133	6
Dynamin-like 120 kDa protein *(A)*	OPA1_RAT	111751	115	5
Mitochondrial fission 1 protein *(C)*	FIS1_RAT	17041	43	1
Dynamin-1-like protein *(A)*	DNM1L_RAT	84369	37	4
Chaperone activity of bc1 complex-like *(C)*	ADCK3_RAT	72750	24	2
Receptor-interacting serine/threonine-protein kinase 3 *(A)*	RIPK3_RAT	52715	24	3
Superoxide dismutase (*A, B, C*)	SODM_RAT	24887	24	1
Protein TBRG4 *(A)*	TBRG4_RAT	71592	24	4
Regulation				
LETM1 and EF-hand domain-containing protein 1 *(C)*	LETM1_RAT	83635	203	10
Elongation factor G *(C)*	EFGM_RAT	84089	96	5
Mitofusin-2 *(C)*	MFN2_RAT	86809	37	4
Thioredoxin-dependent peroxide reductase (*A, B*)	PRDX3_RAT	28563	30	1
Lon protease homolog, mitochondrial (*B,C*)	LONM_RAT	106296	27	9
Single-stranded DNA-binding protein *(A)*	SSBP_RAT	17444	25	1
DNA polymerase subunit gamma-1 *(A)*	DPOG1_RAT	137909	23	3
Others[#]				
Stress-70 protein *(C)*	GRP75_RAT	74097	1023	22
ATP-dependent Clp protease ATP-binding subunit clpX-like *(C)*	CLPX_RAT	69963	288	9
Acyl-coenzyme A thioesterase 2 *(B)*	ACOT2_RAT	49955	178	5
Electron transfer flavoprotein subunit beta *(B)*	ETFB_RAT	27898	145	8
A-kinase anchor protein 1 *(C)*	AKAP1_RAT	92660	95	2
Up-regulated during skeletal muscle growth protein 5 (*A, B*)	USMG5_RAT	6460	92	2
Cytochrome b5 type B (*A, B*)	CYB5B_RAT	16312	89	3
[Pyruvate dehydrogenase [acetyl-transferring]]-phosphatase 1 *(C)*	PDP1_RAT	61739	68	1
Nucleoside diphosphate-linked moiety X motif 19 *(A)*	NUD19_RAT	40426	68	1
Growth hormone-inducible transmembrane protein *(A)*	GHITM_RAT	37324	66	2
[3-methyl-2-oxobutanoate dehydrogenase [lipoamide]] kinase *(C)*	BCKD_RAT	46673	63	1
Iron-sulfur cluster assembly 1 homolog *(C)*	ISCA1_RAT	14311	57	2
ATPase family AAA domain-containing protein 3 (*A, B*)	ATAD3_RAT	66889	53	8
Peroxiredoxin-5 *(B)*	PRDX5_RAT	22507	53	1
Delta(3,5)-Delta(2,4)-dienoyl-CoA isomerase *(A)*	ECH1_RAT	36491	52	2
Tyrosyl-tRNA synthetase, mitochondrial *(C)*	SYYM_RAT	52936	51	1
Quinone oxidoreductase-like protein 2 *(C)*	QORL2_RAT	38095	47	2

Proteins	Uniprot ID	Mass, Da	Score	Peptides
Uncharacterized protein C2orf47 homolog ([A, C])	CB047_RAT	33411	39	1
Transmembrane protein 126A ([A, C])	T126A_RAT	21758	39	3
CDGSH iron-sulfur domain-containing protein 1 [A]	CISD1_RAT	12260	37	1
Brain protein 44 [B]	BR44_RAT	14306	36	2
Coiled-coil domain-containing protein 90B [A]	CC90B_RAT	29895	34	3
ES1 protein homolog ([A, B])	ES1_RAT	28497	34	2
Electron transfer flavoprotein-ubiquinone oxidoreductase [C]	ETFD_RAT	69010	32	5
Glycerol-3-phosphate acyltransferase 1 [C]	GPAT1_RAT	94568	32	2
39S ribosomal protein L14 [C]	RM14_RAT	16017	32	2
Fumarylacetoacetate hydrolase domain-containing protein 1 [C]	FAHD1_RAT	24750	31	1
Kynurenine/alpha-aminoadipate aminotransferase ([A, B, C])	AADAT_RAT	48096	29	2
GTP-binding protein Rhes [B]	RHES_RAT	30576	28	2
Oxidation resistance protein 1 [C]	OXR1_RAT	93209	27	3
Enoyl-CoA hydratase domain-containing protein 3 [B]	ECHD3_RAT	32650	27	4
Protein Mpv17 [C]	MPV17_RAT	19842	27	1
Surfeit locus protein 1 [C]	SURF1_RAT	35060	26	3
RRP15-like protein [A]	RRP15_RAT	31078	26	3
Serine/threonine-protein phosphatase PGAM5 [A]	PGAM5_RAT	32269	25	1
UPF0629 protein C17orf42 homolog [C]	CQ042_RAT	41911	25	1
Leucine-rich PPR motif-containing protein [C]	LPPRC_RAT	157808	24	9
Stomatin-like protein 2 ([A, B])	STML2_RAT	38504	24	1
Growth arrest and DNA damage-inducible proteins-interacting protein 1 [A]	G45IP_RAT	26565	23	7
Probable Xaa-Pro aminopeptidase 3 [A]	XPP3_RAT	57103	23	2
NLR family member X1 [A]	NLRX1_RAT	108548	22	4
Beta-lactamase-like protein 2 [B]	LACB2_RAT	32749	22	1
Translational activator of cytochrome c oxidase 1 [A]	TACO1_RAT	33190	22	5
Pyruvate carboxylase ([A, C])	PYC_RAT	130436	22	4
Kinesin-like protein KIF1B [A]	KIF1B_RAT	205411	21	7
Protein FAM54B [A]	FA54B_RAT	32166	21	2
39S ribosomal protein L38 [C]	RM38_RAT	45095	21	1
Aldehyde dehydrogenase X [B]	AL1B1_RAT	58102	21	1
Patatin-like phospholipase domain-containing protein 7 [A]	PLPL7_RAT	151240	21	1

[A] GST-DEC specific interacting protein (*see* Methods) detected in pulldown samples using mitochondrial lysates from isolated cardiomyocytes;

[B] same as in A but using whole-cell cardiomyocyte lysates;

[C] BK_{Ca}-specific interacting protein detected in immunoprecipitation samples using monoclonal anti-BK_{Ca} antibody and lysates of Percoll purified mitochondria from left ventricle (see Methods).

[D] Grpe1 is equivalent to Mge1 (nucleotide exchange factor of Hsp70).

[(E)] Peptides found (TAVAPIE, YFPTQALNFAFK) are identical in ADP/ATP translocase 1.

[#] Some proteins were re-assigned manually to known functions according to UniProt.

[*] Proteins in “Transport” group were assigned manually. The number of peptides correspond to the highest score of each identified protein.

Table 2

BK_{Ca} channel-interacting proteins from identified by LC/MS/MS.

Proteins	Uniprot ID	Mass, Da	Score	Peptides
Endoplasmic Reticulum				
Extended synaptotagmin-1 (*B,C*)	ESYT1_RAT	121369	139	6
78 kDa glucose-regulated protein (*B,C*)	GRP78_RAT	72473	136	4
Sarcoplasmic/endoplasmic reticulum calcium ATPase 1 (*A, B,C*)	AT2A1_RAT	110707	65	2
Carnitine O-acetyltransferase (*A, C*)	CACP_RAT	71211	65	4
Erlin-2 (*B*)	ERLN2_RAT	37915	62	4
Elongation factor 1-gamma (*A,B*)	EF1G_RAT	50371	57	3
Serpin H1 (*B*)	SERPH_RAT	46602	51	3
Cytochrome P450 2C11 (*A*)	CP2CB_RAT	57658	39	3
Calreticulin (*A*)	CALR_RAT	48137	38	1
Dolichyl-diphosphooligosaccharide--protein glycosyltransferase subunit 2 (*B*)	RPN2_RAT	69149	37	2
Sterol regulatory element-binding protein 2 (*A, C*)	SRBP2_RAT	124096	37	2
Calnexin (*A, B*)	CALX_RAT	67612	36	2
ORM1-like protein 3 (*C*)	ORML3_RAT	17451	34	1
Reticulon-4 (*C*)	RTN4_RAT	126766	33	3
Antigen peptide transporter 2 (*A*)	TAP2_RAT	78063	32	3
Procollagen-lysine,2-oxoglutarate 5-dioxygenase 3 (*A*)	PLOD3_RAT	85577	31	2
Cytochrome P450 2A2 (*A*)	CP2A2_RAT	56480	30	3
3 beta-hydroxysteroid dehydrogenase/Delta 5-->4-isomerase type 2 (*A*)	3BHS2_RAT	42592	29	1
HCLS1-associated protein X-1 (*C*)	HAX1_RAT	31429	29	2
Inositol 1,4,5-trisphosphate receptor type 1 (*A, C*)	ITPR1_RAT	316486	29	3
Transmembrane protein 214 (*A*)	TM214_RAT	77486	29	2
Sterol-4-alpha-carboxylate 3-dehydrogenase, decarboxylating (*A*)	NSDHL_RAT	40671	27	1
Squalene synthase (*A*)	FDFT_RAT	48703	26	1
Protein ERGIC-53-like (*A*)	LMA1L_RAT	56571	26	2
BET1 homolog (*A*)	BET1_RAT	13336	26	2
Protein ERGIC-53 (*B*)	LMAN1_RAT	58206	26	1
Cytochrome P450 3A1 (*B*)	CP3A1_RAT	58222	26	1
Carboxylesterase 3 (*B*)	CES3_RAT	62393	25	2
Choline-phosphate cytidylyltransferase B (*B*)	PCY1B_RAT	42159	25	1
Reticulocalbin-2 (*A*)	RCN2_RAT	37410	25	2
Cytochrome P450 2C12, female-specific (*C*)	CP2CC_RAT	56453	24	1

Proteins	Uniprot ID	Mass, Da	Score	Peptides
Cytochrome P450 2E1 ([C])	CP2E1_RAT	56990	24	2
Multiple coagulation factor deficiency protein 2 homolog ([A])	MCFD2_RAT	16252	24	1
Thrombospondin-4 ([A])	TSP4_RAT	110882	24	1
DnaJ homolog subfamily C member 3 ([A,C])	DNJC3_RAT	57981	24	3
Lipase maturation factor 2 ([A])	LMF2_RAT	80431	23	1
Phosphatidylinositol-glycan biosynthesis class W protein ([A,C])	PIGW_RAT	57205	23	1
LDLR chaperone MESD ([A])	MESD_RAT	25314	23	1
Uncharacterized glycosyltransferase AER61 ([C])	AER61_RAT	62340	23	2
Inhibitor of nuclear factor kappa-B kinase-interacting protein ([B])	IKIP_RAT	42391	22	3
Sphingosine-1-phosphate lyase 1 ([A])	SGPL1_RAT	64287	22	4
Dehydrogenase/reductase SDR family member 7B ([C])	DRS7B_RAT	35662	22	2
UDP-glucose:glycoprotein glucosyltransferase 1 ([C])	UGGG1_RAT	177061	22	3
Poly [ADP-ribose] polymerase 16 ([C])	PAR16_RAT	37088	21	2
Golgi				
Ras-related protein Rab-10 ([C])	RAB10_RAT	23072	102	2
Ras-related protein Rab-1A ([C])	RAB1A_RAT	22891	67	2
Calcium-transporting ATPase type 2C member 1 ([B])	AT2C1_RAT	101519	39	2
Nucleobindin-2 ([A])	NUCB2_RAT	50173	39	1
Phosphofurin acidic cluster sorting protein 1 ([A, B])	PACS1_RAT	105034	32	2
Golgin subfamily A member 2 ([A])	GOGA2_RAT	113232	31	7
Caveolin-3 ([A), B])	CAV3_RAT	17904	31	1
CMP-N-acetylneuraminate-beta-1,4-galactoside alpha-2,3-sialyltransferase ([A])	SIAT6_RAT	42340	29	3
Protein O-linked-mannose beta-1,2-N-acetylglucosaminyltransferase 1 ([A])	PMGT1_RAT	75670	28	1
Alpha-1,3-mannosyl-glycoprotein 2-beta-N-acetylglucosaminyltransferase ([A])	MGAT1_RAT	51839	27	1
Myomegalin ([A, B,C])	MYOME_RAT	263193	26	7
Vacuolar protein sorting-associated protein 54 ([B])	VPS54_RAT	109913	24	3
Acid phosphatase-like protein 2 ([C])	ACPL2_RAT	55664	24	1
Golgi phosphoprotein 3-like ([A])	GLP3L_RAT	33072	23	3
Carbohydrate sulfotransferase 11 ([B])	CHSTB_RAT	42112	23	3
Beta-1,4-mannosyl-glycoprotein 4-beta-N-acetylglucosaminyltransferase ([A])	MGAT3_RAT	62552	22	1
Golgi SNAP receptor complex member 2 ([B])	GOSR2_RAT	24649	21	1
Nucleus				
Vimentin ([A, B,C])	VIME_RAT	53757	942	16

Proteins	Uniprot ID	Mass, Da	Score	Peptides
Alpha-actinin-4 ([A, B,C])	ACTN4_RAT	105306	319	18
Keratin, type I cytoskeletal 13 ([A, C])	K1C13_RAT	48098	208	9
Lamin-B1 ([A])	LMNB1_RAT	66794	126	7
Caveolin-2 ([B])	CAV2_RAT	18482	124	1
Histone H2A type 1-C ([A])	H2A1C_RAT	14097	123	2
Cullin-associated NEDD8-dissociated protein 2 ([A])	CAND2_RAT	141238	117	4
60S ribosomal protein L23a ([A, C])	RL23A_RAT	17684	104	1
Homeobox protein Nkx-6.1 ([A, B,C])	NKX61_RAT	37723	89	1
Cyclin-dependent kinase 7 (Fragment) ([A])	CDK7_RAT	37402	59	2
DNA-directed RNA polymerase I subunit RPA1 ([A, B,C])	RPA1_RAT	196235	54	3
Centrosomal protein of 57 kDa ([A, C])	CEP57_RAT	57404	49	4
Heterogeneous nuclear ribonucleoproteins A2/B1 ([A])	ROA2_RAT	37512	49	1
Serine/threonine-protein kinase TNNI3K ([A, B])	TNI3K_RAT	93985	44	1
Mitotic spindle assembly checkpoint protein MAD2B ([A, B])	MD2L2_RAT	24615	39	1
Speckle targeted PIP5K1A-regulated polyA polymerase ([A])	STPAP_RAT	95516	38	2
Myc-induced nuclear antigen ([A])	MINA_RAT	53638	37	2
DNA mismatch repair protein Msh2 ([A])	MSH2_RAT	104704	37	5
Snurportin-1 ([A])	SPN1_RAT	41337	37	1
Transcription initiation factor TFIID subunit 6 ([A])	TAF6_RAT	73295	36	1
Ras association domain-containing protein 2 ([B])	RASF2_RAT	38168	36	1
60S ribosomal protein L11 ([A])	RL11_RAT	20468	36	1
Serine/threonine-protein kinase MAK ([A, C])	MAK_RAT	70280	35	1
Tyrosine-protein kinase Fer (Fragment) ([A])	FER_RAT	37479	35	2
Coiled-coil and C2 domain-containing protein 1B ([A])	C2D1B_RAT	93818	34	3
Splicing regulatory glutamine/lysine-rich protein 1 ([C])	SREK1_RAT	56930	34	3
Zinc finger protein 57 ([A])	ZFP57_RAT	47584	34	2
UPF0027 protein C22orf28 homolog ([A])	CV028_RAT	55727	33	1
Scaffold attachment factor B1 ([A, B,C])	SAFB1_RAT	104960	33	4
Transmembrane protein 109 ([A,B])	TM109_RAT	26282	33	2
DNA topoisomerase 1 ([A, C])	TOP1_RAT	91159	32	3
Hypoxia-inducible factor 3-alpha ([A])	HIF3A_RAT	73470	32	1
Nucleoporin GLE1 ([A])	GLE1_RAT	79955	31	4
Double-stranded RNA-specific editase 1 ([A])	RED1_RAT	78218	31	2
Doublesex- and mab-3-related transcription factor C1 ([A])	DMRTC_RAT	24055	31	2
Origin recognition complex subunit 1 ([C])	ORC1_RAT	96840	30	2
5′-AMP-activated protein kinase subunit gamma-1 ([A])	AAKG1_RAT	37534	30	1

Proteins	Uniprot ID	Mass, Da	Score	Peptides
Transforming growth factor beta regulator 1 ([A, C])	TBRG1_RAT	45384	30	2
High mobility group nucleosome-binding domain-containing protein 3 ([C])	HMGN3_RAT	10176	30	1
Histone acetyltransferase MYST2 ([C])	MYST2_RAT	71154	30	2
Zinc finger and BTB domain-containing protein 44 ([A, B])	ZBT44_RAT	50987	30	3
DNA (cytosine-5)-methyltransferase 1 ([A, B])	DNMT1_RAT	185054	30	5
Nasal embryonic luteinizing hormone-releasing hormone factor ([A])	NELF_RAT	60701	30	4
Zinc finger and BTB domain-containing protein 24 ([A])	ZBT24_RAT	79355	29	3
Nuclear pore complex protein Nup155 ([A, B])	NU155_RAT	156387	29	2
Period circadian protein homolog 2 ([B])	PER2_RAT	137539	28	2
Far upstream element-binding protein 2 ([A, B])	FUBP2_RAT	74466	28	1
Paired box protein Pax-8 ([A])	PAX8_RAT	49118	28	1
Coiled-coil domain-containing protein 55 ([C])	CCD55_RAT	64370	28	2
PIN2/TERF1-interacting telomerase inhibitor 1 ([A])	PINX1_RAT	36916	28	2
Coiled-coil domain-containing protein KIAA1826 homolog ([A])	K1826_RAT	41264	28	1
Probable ATP-dependent RNA helicase DDX46 ([A, C])	DDX46_RAT	117826	28	6
Lethal(3)malignant brain tumor-like protein 2 ([A])	LMBL2_RAT	80057	28	1
DNA-directed RNA polymerase III subunit RPC3 ([A])	RPC3_RAT	60903	27	2
DNA polymerase delta catalytic subunit ([A])	DPOD1_RAT	124948	27	5
Nuclear pore complex protein Nup54 ([A, C])	NUP54_RAT	55825	27	1
ATP-dependent RNA helicase DDX39 ([A])	DDX39_RAT	49591	27	4
Histone deacetylase 4 ([A, C])	HDAC4_RAT	119377	27	3
DNA topoisomerase 2-alpha ([A])	TOP2A_RAT	173853	27	6
PDZ domain-containing protein 2 ([A, C])	PDZD2_RAT	296389	27	4
Coiled-coil domain-containing protein 104 ([A])	CC104_RAT	39736	27	2
Neurofibromin ([C])	NF1_RAT	320473	27	1
Forkhead box protein J1 ([C])	FOXJ1_RAT	45994	27	2
Origin recognition complex subunit 2 ([A])	ORC2_RAT	66094	27	3
Transcriptional adapter 2-alpha ([A, B])	TAD2A_RAT	52107	27	2
Telomerase protein component 1 ([A, B,C])	TEP1_RAT	295173	26	5
Transcription factor EC ([A, C])	TFEC_RAT	35495	26	2
SAP domain-containing ribonucleoprotein ([A])	SARNP_RAT	23647	26	2
Transcription elongation factor A protein-like 8 ([A])	TCAL8_RAT	13553	26	1
Protein AATF ([A])	AATF_RAT	59461	26	2
DNA-directed RNA polymerase I subunit RPA2 ([A])	RPA2_RAT	129462	26	2
Zinc finger CCCH domain-containing protein 18 ([C])	ZCH18_RAT	105702	26	2

Proteins	Uniprot ID	Mass, Da	Score	Peptides
Transcription factor AP-2-alpha (A, C)	AP2A_RAT	48316	26	3
Neuronal PAS domain-containing protein 4 (C)	NPAS4_RAT	88004	26	1
Clusterin-associated protein 1 (B)	CLUA1_RAT	46543	26	2
Apolipoprotein A-IV (A)	APOA4_RAT	44429	25	1
60S ribosomal protein L3 (A), B)	RL3_RAT	46392	25	4
40S ribosomal protein S13 (A)	RS13_RAT	17212	25	2
Phosphatase and actin regulator 3 (A, B)	PHAR3_RAT	58596	25	2
Histone H3.3 (A)	H33_RAT	15376	25	2
SKI family transcriptional corepressor 1 (A)	SKOR1_RAT	101312	25	3
Protein GRINL1A (A, B)	GRL1A_RAT	41305	25	1
Cell growth-regulating nucleolar protein (A, C)	LYAR_RAT	44110	25	2
Pancreas/duodenum homeobox protein 1 (C)	PDX1_RAT	30983	25	1
DNA repair protein RAD50 (A, C)	RAD50_RAT	154772	25	15
RAC-gamma serine/threonine-protein kinase (B)	AKT3_RAT	56217	25	2
Leucine-rich repeat flightless-interacting protein 1 (C)	LRRF1_RAT	80484	25	2
Something about silencing protein 10 (C)	SAS10_RAT	53949	24	1
Structural maintenance of chromosomes protein 3 (A, B,C)	SMC3_RAT	138761	24	4
MACRO domain-containing protein 1 (Fragment) (C)	MACD1_RAT	29081	24	2
ZW10 interactor (C)	ZWINT_RAT	30295	24	3
Protein Dom3Z (A, C)	DOM3Z_RAT	45784	24	2
Kazrin (C)	KAZRN_RAT	87433	24	3
General transcription factor 3C polypeptide 1 (A, B,C)	TF3C1_RAT	245004	24	3
Suppression of tumorigenicity 18 protein (A)	ST18_RAT	115074	24	2
Myocyte-specific enhancer factor 2A (A)	MEF2A_RAT	53391	24	2
Homeobox protein MOX-2 (A)	MEOX2_RAT	33869	24	1
Ubiquitin carboxyl-terminal hydrolase 16 (A)	UBP16_RAT	95242	24	3
Sentrin-specific protease 2 (A)	SENP2_RAT	67837	24	1
Far upstream element-binding protein 1 (A, B)	FUBP1_RAT	67326	24	3
Hepatoma-derived growth factor-related protein 2 (A)	HDGR2_RAT	74088	24	1
1-phosphatidylinositol-4,5-bisphosphate phosphodiesterase beta-1 (A)	PLCB1_RAT	139113	24	1
Selenocysteine insertion sequence-binding protein 2 (A,B,C)	SEBP2_RAT	94154	24	5
Protein salvador homolog 1 (B)	SAV1_RAT	45133	24	3
Structural maintenance of chromosomes protein 1A (A)	SMC1A_RAT	143743	23	5
DNA-binding protein SMUBP-2 (A)	SMBP2_RAT	109400	23	3
Myocyte-specific enhancer factor 2D (A, B)	MEF2D_RAT	54563	23	3

Proteins	Uniprot ID	Mass, Da	Score	Peptides
Nuclear pore membrane glycoprotein 210 ([A, B])	PO210_RAT	204943	23	2
Myb-binding protein 1A ([A])	MBB1A_RAT	153046	23	4
Fidgetin-like protein 1 ([A])	FIGL1_RAT	74891	23	1
Smad nuclear interacting protein 1 ([A])	SNIP1_RAT	44953	23	1
Aryl hydrocarbon receptor nuclear translocator 2 ([A])	ARNT2_RAT	78536	23	1
H/ACA ribonucleoprotein complex subunit 1 ([A, B])	GAR1_RAT	23167	23	1
Putative rRNA methyltransferase 3 ([A, B,C])	RRMJ3_RAT	95165	23	2
REST corepressor 2 ([C])	RCOR2_RAT	58116	23	1
PR domain zinc finger protein 2 ([C])	PRDM2_RAT	189890	23	2
MutS protein homolog 5 ([B,C])	MSH5_RAT	93362	23	2
E3 SUMO-protein ligase PIAS3 ([C])	PIAS3_RAT	69289	23	1
Transcription factor IIIB 50 kDa subunit ([C])	BRF2_RAT	47421	22	2
6-phosphofructo-2-kinase/fructose-2,6-biphosphatase 3 ([C])	F263_RAT	64491	22	1
Vitamin D3 receptor ([B])	VDR_RAT	48467	22	2
Meiosis-specific nuclear structural protein 1 ([A, B])	MNS1_RAT	61316	22	5
Cell division cycle-associated protein 7 ([A])	CDCA7_RAT	43909	22	2
Kinesin-like protein KIF22 ([A, C])	KIF22_RAT	73239	22	5
Protein timeless homolog ([A])	TIM_RAT	139562	22	4
U11/U12 small nuclear ribonucleoprotein 35 kDa protein ([A])	U1SBP_RAT	29186	22	2
Nuclear pore complex protein Nup85 ([A, B])	NUP85_RAT	29186	22	2
Interferon-stimulated 20 kDa exonuclease-like 2 ([A])	I20L2_RAT	41684	22	3
ATPase WRNIP1 ([A])	WRIP1_RAT	72687	22	2
Nucleolar RNA helicase 2 ([A])	DDX21_RAT	86540	22	4
Period circadian protein homolog 1 ([A, B])	PER1_RAT	137562	22	2
U4/U6.U5 tri-snRNP-associated protein 1 ([A, B,C])	SNUT1_RAT	91127	22	2
Intraflagellar transport protein 172 homolog ([C])	IF172_RAT	199245	22	2
Serine/threonine-protein kinase PRP4 homolog ([A])	PRP4B_RAT	117335	22	3
CLK4-associating serine/arginine rich protein ([C])	CLASR_RAT	76932	22	3
Nuclear pore complex protein Nup98-Nup96 ([A])	NUP98_RAT	198358	21	1
Nucleolar GTP-binding protein 1 ([A])	NOG1_RAT	74640	21	3
Protein SCAF8 ([A])	SCAF8_RAT	139874	21	2
Myogenin ([A, B,C])	MYOG_RAT	33224	21	2
Ester hydrolase C11orf54 homolog ([C])	CK054_RAT	35427	21	2
Uncharacterized protein C1orf103 homolog ([C])	CA103_RAT	83074	21	4
Poly(ADP-ribose) glycohydrolase ([A, B])	PARG_RAT	110417	21	1
Dual specificity protein kinase CLK3 ([C])	CLK3_RAT	59247	21	2

Proteins	Uniprot ID	Mass, Da	Score	Peptides
Scm-like with four MBT domains protein 1 ([A, B,C])	SMBT1_RAT	98984	21	1
Chromodomain-helicase-DNA-binding protein 8 ([A, B,C])	CHD8_RAT	292449	21	1
Digestive organ expansion factor homolog ([C])	DEF_RAT	88169	21	2
Uncharacterized protein C12orf32 homolog ([C])	CL032_RAT	27281	21	1
Regulator of G-protein signaling 14 ([C])	RGS14_RAT	59968	21	1
Zinc finger CCHC-type and RNA-binding motif-containing protein 1 ([C])	ZCRB1_RAT	24758	21	2
Spliceosome RNA helicase Bat1 ([B])	UAP56_RAT	49460	21	1
E3 SUMO-protein ligase PIAS2 ([B])	PIAS2_RAT	64303	21	1

[A] GST-DEC specific interacting protein (*see* Methods) detected in pulldown samples using mitochondrial lysates from isolated cardiomyocytes.;

[B] same as in A but using whole-cell cardiomyocyte lysates;

[C] BK_{Ca} specific interacting protein (see Methods) detected in immunoprecipitation samples using monoclonal anti-BK_{Ca} antibody and lysates of Percoll purified mitochondria from left ventricle.